COOPERATION

CANADA- NOVA SCOTIA
COOPERATION
AGREEMENT ON MINERAL
DEVELOPMENT

ENTENTE DE
COOPÉRATION CANADA-
NOUVELLE-ÉCOSSE
SUR L'EXPLOITATION
MINÉRALE

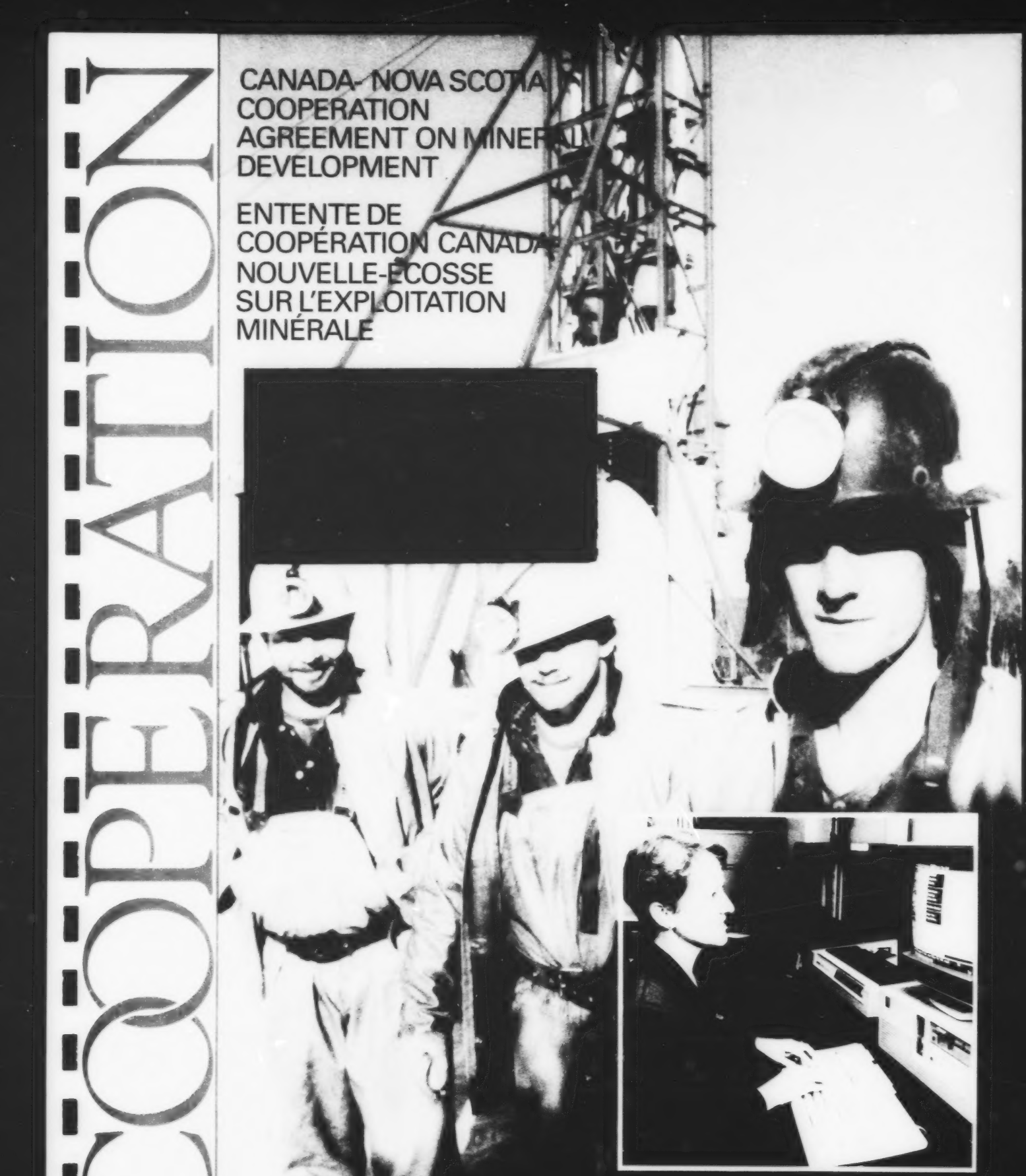

Nova Scotia

OPEN FILE REPORT 92-009

Mineralogical Investigations along the Upper Seal Harbour Antimony Line, Goldboro, Nova Scotia

M. C. Corey

Nova Scotia Department of Natural Resources

Honourable John G. Leefe, Minister

Halifax, Nova Scotia
1992

COOPERATION

COOPERATION AGREEMENT ON MINERAL DEVELOPMENT

ENTENTE DE COOPÉRATION SUR LE DÉVELOPPEMENT DES MINÉRAUX

Canada and Nova Scotia, Working for a Stronger Mineral Industry

Canada

Nova Scotia

93-00815/

MINERALOGICAL INVESTIGATIONS ALONG THE UPPER SEAL HARBOUR ANTICLINE, GOLDBORO, NOVA SCOTIA

M. C. Corey

INTRODUCTION

The Goldboro project has focused on several aspects of gold mineralization along the Upper Seal Harbour anticline in the Goldboro area. Study areas included the Boston-Richardson, East and West Gold Brook Mines and the Dolliver Mountain Mine. Historically, the most profitable of these was the Boston-Richardson Mine which produced 53,835 oz. of gold at an average grade of 0.136 oz./ton. Gold production ceased in 1912 (Malcolm, 1976).

The Upper Seal Harbour anticline trends east-west at 95° with a variable eastward plunge at 10-35°. The axial surface dips 85° to the south. Strata on the limbs of the anticline dip steeply from 65-75° north and south. Mineralization is hosted by en echelon and less common, bedding parallel, quartz veins situated along the anticline fold hinge. The en echelon veins are stratabound but irregular and are hosted by massive to interbedded grey to black pelite and semi-pelite; together the quartz and host-rock packages are referred to as belts. The occurrence of black pelite appears to be restricted to the immediate fold hinge area. The belts reflect upper greenschist to lower amphibolite facies metamorphism and range in thickness from < 10 cm to approximately 2 m. The amount of veining within the belts is highly variable ranging from minor to 100%. Gold occurs as millimetre-sized grains in massive milky quartz to micron-sized inclusions within vein- and wall rock-hosted sulphides (Parent, 1989).

Several aspects of the mineralization were investigated as part of the current study. This work includes: (1) establishing the mineralogy and mineral chemistry of both veins and host rocks, (2) the types and styles of alteration and (3) documenting the various structural features present. Four periods of deformation have been recognized from mapping. Also present near the fold hinge are a series of kink bands which trend southwest (145°) dip 45° northwest and plunge at 40°.

GENERAL GEOLOGY

Figure 1 shows the distribution of gold deposits within the eastern half of the Meguma Terrane relative to the regional geology. Also shown are northwest-trending, high angle, brittle-ductile faults which are present at many Meguma Group gold deposits. These faults vary in length from tens of metres to tens of kilometers and movement along them is generally sinistral (Williams and Hy, 1990). These faults manifest themselves on a local scale as shear and breccia zones.

Gold mineralization in the Goldboro area is situated along the fold axis of several anticlines (see Fig.2) located within Cambrian to Ordovician metasediments of the Meguma Group. These anticlines trend roughly east-west and generally have tight, upright geometry. The surrounding area, specifically Country Harbour to New Harbour (Fig. 2) is underlain by psammites, semi-pelites and pelites belonging to the Goldenville and the conformably overlying Halifax Formations respectively. These in turn have been intruded by several small peraluminous granitic plutons. In this area the Meguma Group reflects both regional deformation (Table 1) and metamorphism, characterized by; (1) east-west trending folds, (2) axial-planar slaty and pressure solution cleavages (S_2), (3) later syn-plutonic subhorizontal crenulation cleavage (S_3) which is best developed within semi-pelite, and (4) later upright shear cleavage (S_{4-5}) and kink-banding as a result of brittle-ductile shearing and faulting (Keppie, 1983: O'Brien, 1983; Haynes, 1983). Regional metamorphism ranges from greenschist-facies

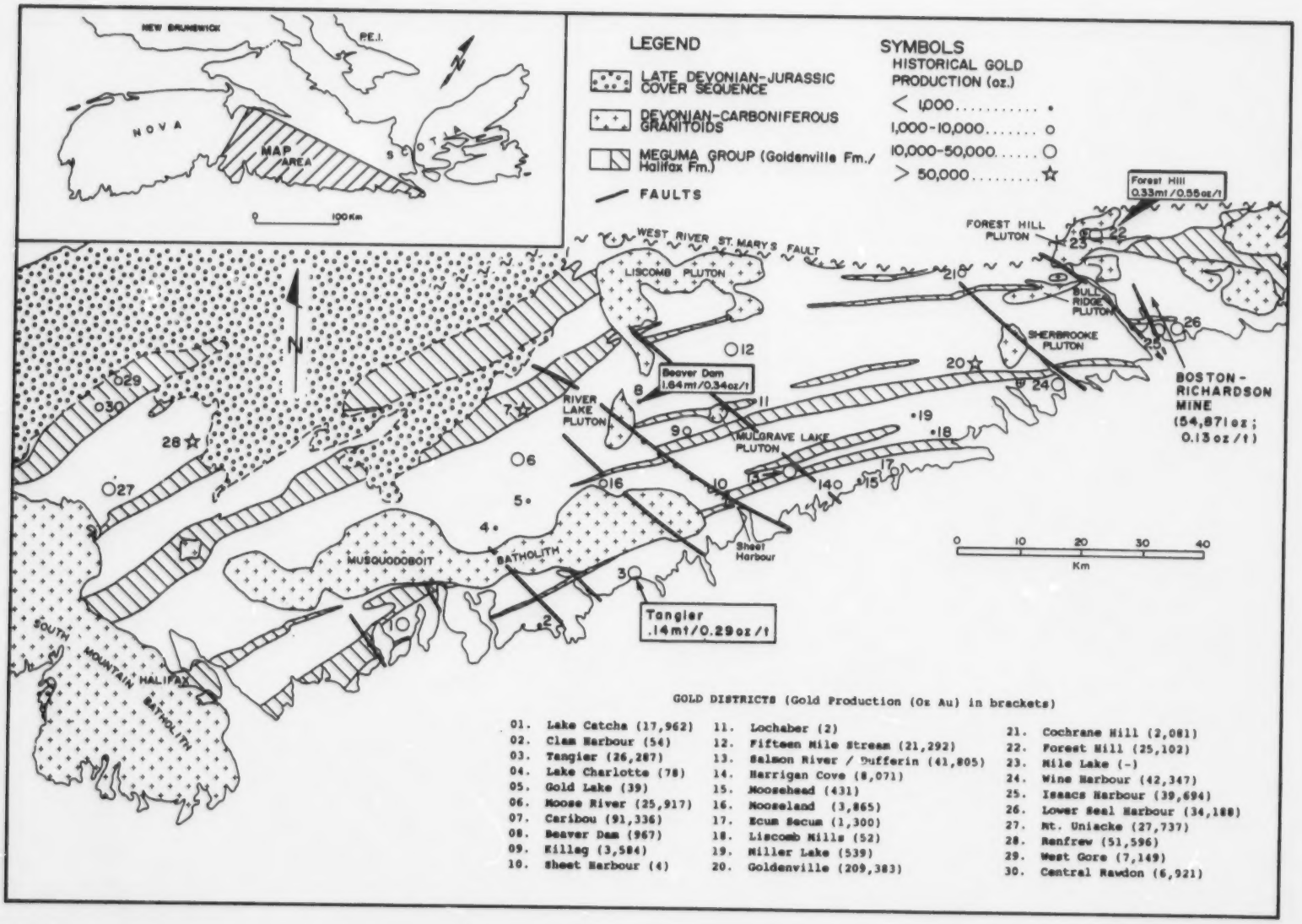

FIGURE 1. General geology of the eastern Meguma Terrane.

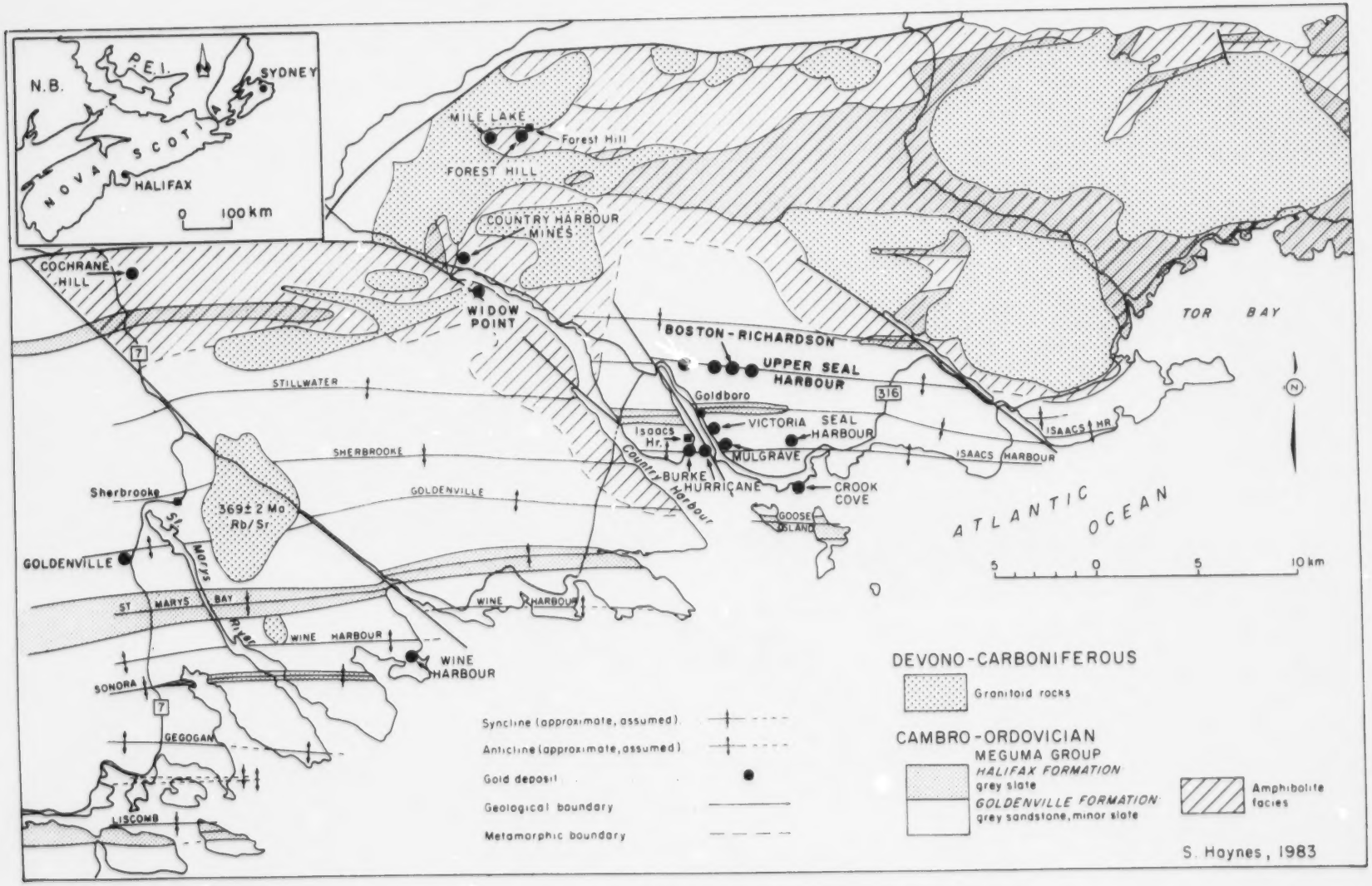

FIGURE 2. Geology map of a portion of the eastern Meguma Terrane showing the distribution of metamorphic facies and gold deposits. Modified from Haynes (1983).

TABLE 1. Structural elements observed within the eastern Meguma Terrane (modified after Smith, 1988).

DEFORMATION	*CHARACTERISTIC FEATURES*	*COMMENTS*
D_1	*rare folds, grain alignment cleavage (flat; folded steep)*	*variably developed throughout the Eastern Meguma Zone.*
D_2	*pervasive regional folds; upright slatey and pressure solution cleavages; pre-regional metamorphism*	*generally transposed into parallelism with S_4 cleavage on fold limbs.*
----------*METAMORPHISM*----------		
D_3	*controlled by lithology; no folds; coarse grained biotite foliation; syn- plutonism at ~370 M.Y.A.*	*subhorizontal orientation except where it is steepened in D_4 shear zones.*
----------*PLUTONISM*----------		
D_4	*associated with ductile shear upright cleavage; deforms metamorphic porphyroblasts.*	*shear zones; may locally be confused with S_2 slatey cleavage.*
D_5	*crenulations; faults (thrust, reverse, normal, strike slip) kink bands, boudinage.*	*includes all post D_4 brittle/ ductile structures.*

within the Goldboro area to amphibolite-facies immediately to the north in the area of Country Harbour Mines and Forest Hill, reflecting contact metamorphism associated with plutonism (Fig. 2). Amphibolite-grade metamorphism has also been noted east and west of Goldboro associated with the north-west trending, sinistral New Harbour and Country Harbour faults respectively. Amphibolite-grade rocks are characterized by; biotite + garnet ± cordierite ± staurolite (Douma, in prep). In the area of gold deposition these regional features have been overprinted by the effects of local alteration and metamorphism associated with gold mineralization, ca.370 my. (Smith and Kontak, 1987; Smith and Kontak, 1988b). A much more comprehensive discussion of the geology and structure of this area is provided by Keppie (1983), Haynes (1983), O'Brien(1983) and Smith (1983).

The site of recent exploration and development work by Exploration Orex Inc. which on the area of the historical Boston-Richarson mine is situated on the fold axis of the Upper Seal Harbour anticline (Fig.2). The anticline can be traced from Country Harbour eastward to New Harbour, a distance of approximately 40km. The Upper Seal Harbour anticline is also host to several other gold deposits in the Goldboro area. These are, to the west of the Boston-Richardson mine, the West Gold Brook and Dolliver Mountain mines and to the east, the East Gold Brook mine (Fig. 3). Although geologically similar to the Boston-Richardson mine (see below) these deposits have no significant historical gold production. The Upper Seal Harbour anticline trends approximately 95° with a variable eastward plunge from near horizontal where exposed along Isaacs Harbour River west of Dolliver Mountain, to 10° at Dolliver Mountain, to 32° in the Boston-Richardson mine. The anticline is also reported to be more sharply folded at Dolliver Mountain than at the Boston-Richardson mine. Over the same strike length, the axial plane dips to the south 85-86° and the limbs dip steeply 65-75°. A change in the dip of the axial plane to slightly north dipping was noted within the original Boston-Richardson below the 400ft. level.

GEOLOGY OF THE BOSTON-RICHARDSON MINE

The following description is based predominately on the observations of Exploration Orex Inc. geologists during extensive diamond drilling and underground development.

Disseminated gold mineralization consisting of native gold, auriferous arsenopyrite and galena, and gold-bismuth tellurides (see below) occur associated with arsenopyrite + galena ± pyrrhotite ± chalcopyrite ± sphalerite within thick, massive quartz veins hosted by discrete black, graphitic pelite and semi-pelite beds separated by thick psammite beds. Gold may also be found within the wall rocks associated with abundant arsenopyrite and minor pyrite, pyrrhotite and chalcopyrite. The entire gold-bearing quartz and host-rock package has been referred to as a belt. To date there have been fourteen such belts (referred to as N_1-N_{14}) indentified beneath the original Richardson belt (Fig. 4). The total thickness of this package is approximately 100m on the limbs to >300m at the fold axis. This is consistent with observations during mining of the Richardson belt where it was shown to increase in thickness from 2.5m on the limbs to 6m at the fold axis. Lying stratigraphically between the N series of quartz belts and the Richardson belt at the fold axis is a 40m thick marker unit consisting of interbedded semi-pelite and psammite unit containing rare gold within an extensive quartz stockwork as well as minor AC veins. Above the Richardson belt, to the east and south of the fold axis in the area of the East Gold Brook mine, are additional gold-bearing quartz veins within a semi-pelite ± interlaminated pelite package.

Several types of auriferous quartz veins occur within the Boston-Richardson mine. These include; 1) typical crack-seal textured, bedding parallel veins, 2) discordant massive white en echelon veins, 3) oblique shear veins and 4) high angle AC veins (Plate 1a-d). Quartz veining appears to have been multistage and all types may occur within a particular belt where they may comprise up to 100% of the belt (Fig. 5; Plate 2). In contrast to many Meguma-hosted gold deposits (e.g. Tangier) where crack-seal textured bedding parallel veins are the

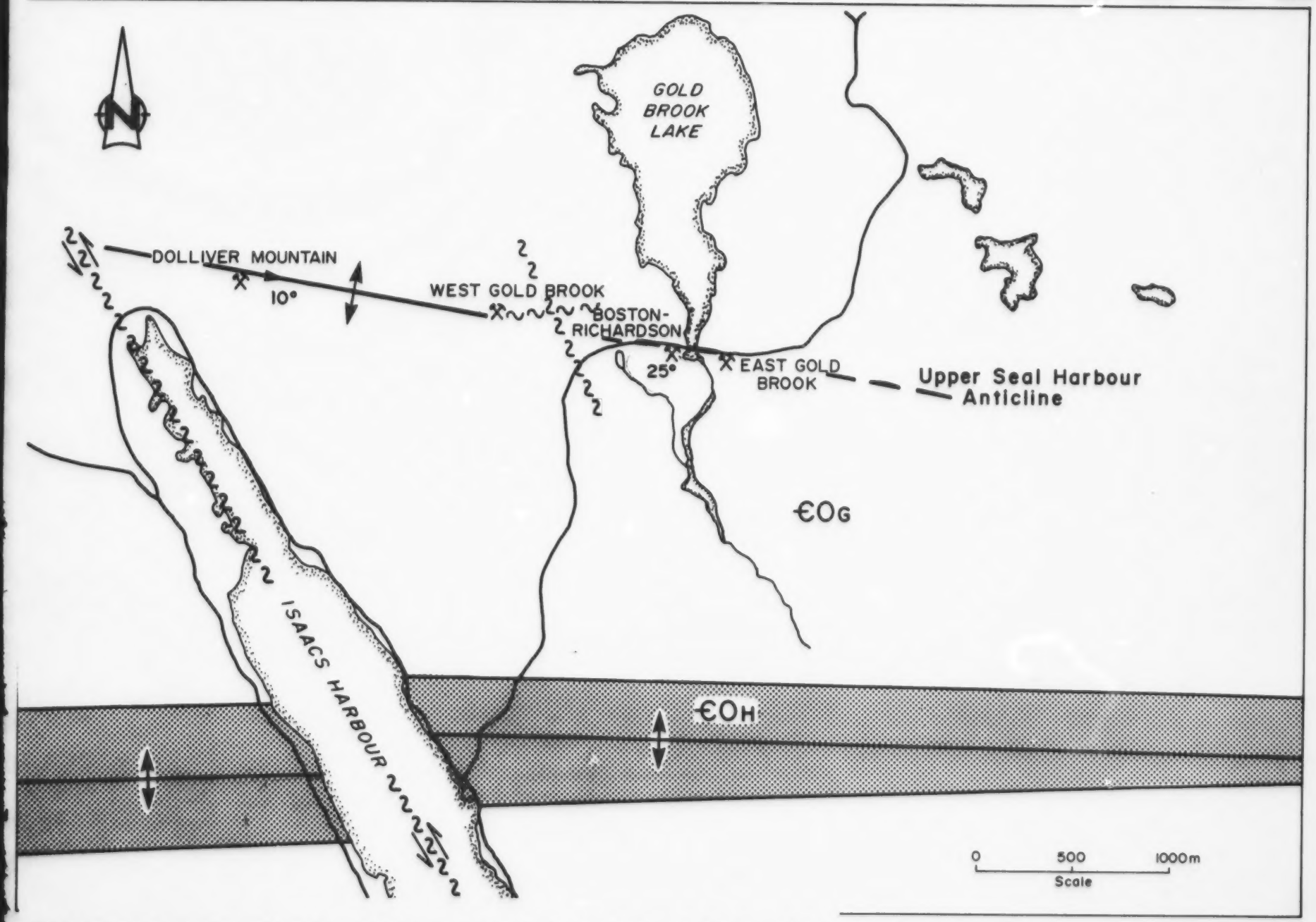

FIGURE 3. Detail geology map of the study area showing location of gold deposits along the Upper Seal Harbour anticline.

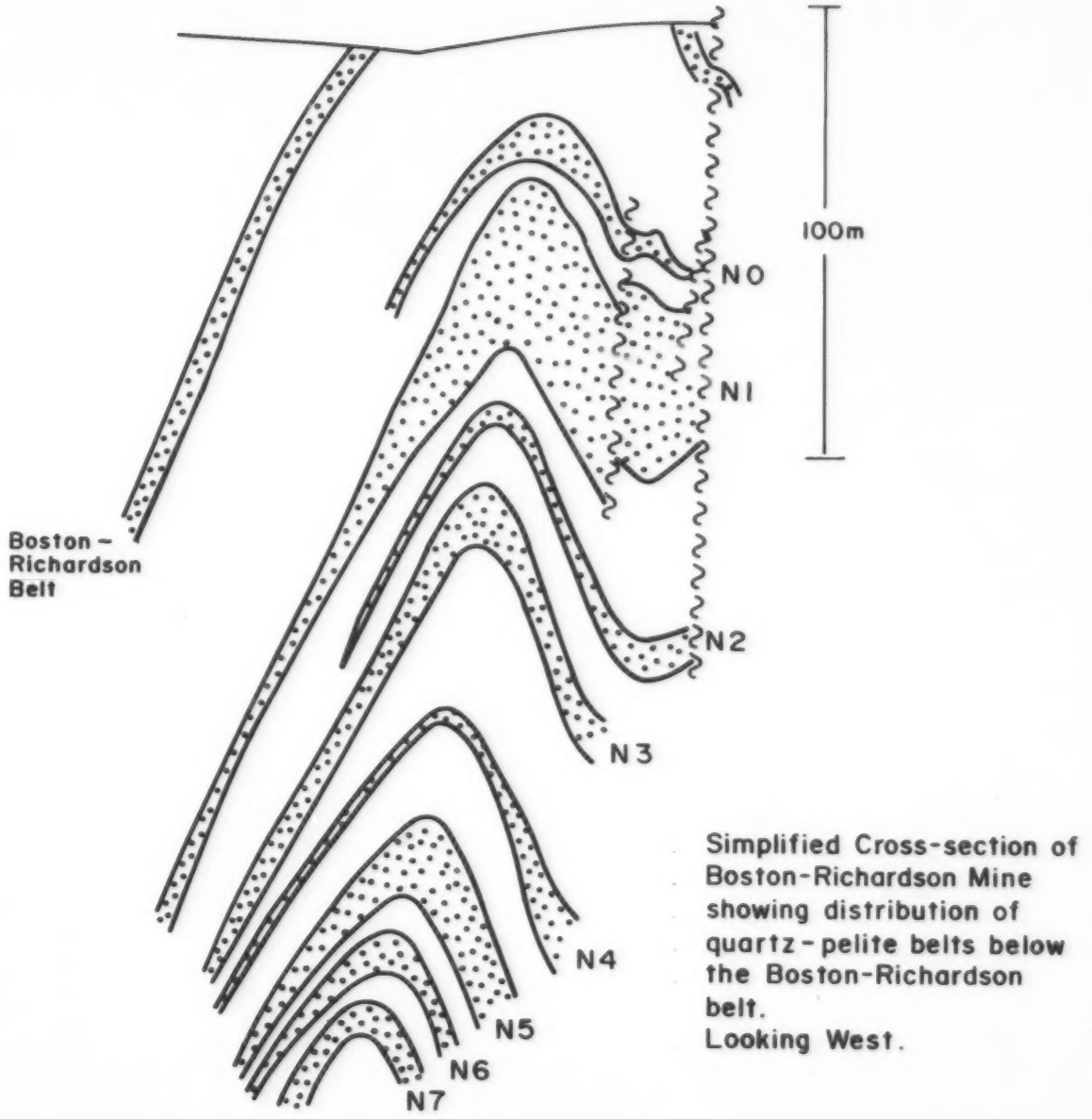

FIGURE 4. Exploration Orex Inc. section showing distribution of quartz belts within the Boston-Richardson mine. The amount of quartz within the belts is highly variable. To date 15 quartz belts have been delineated beneath the Boston-Richardson. From Parent and Ethier (1989).

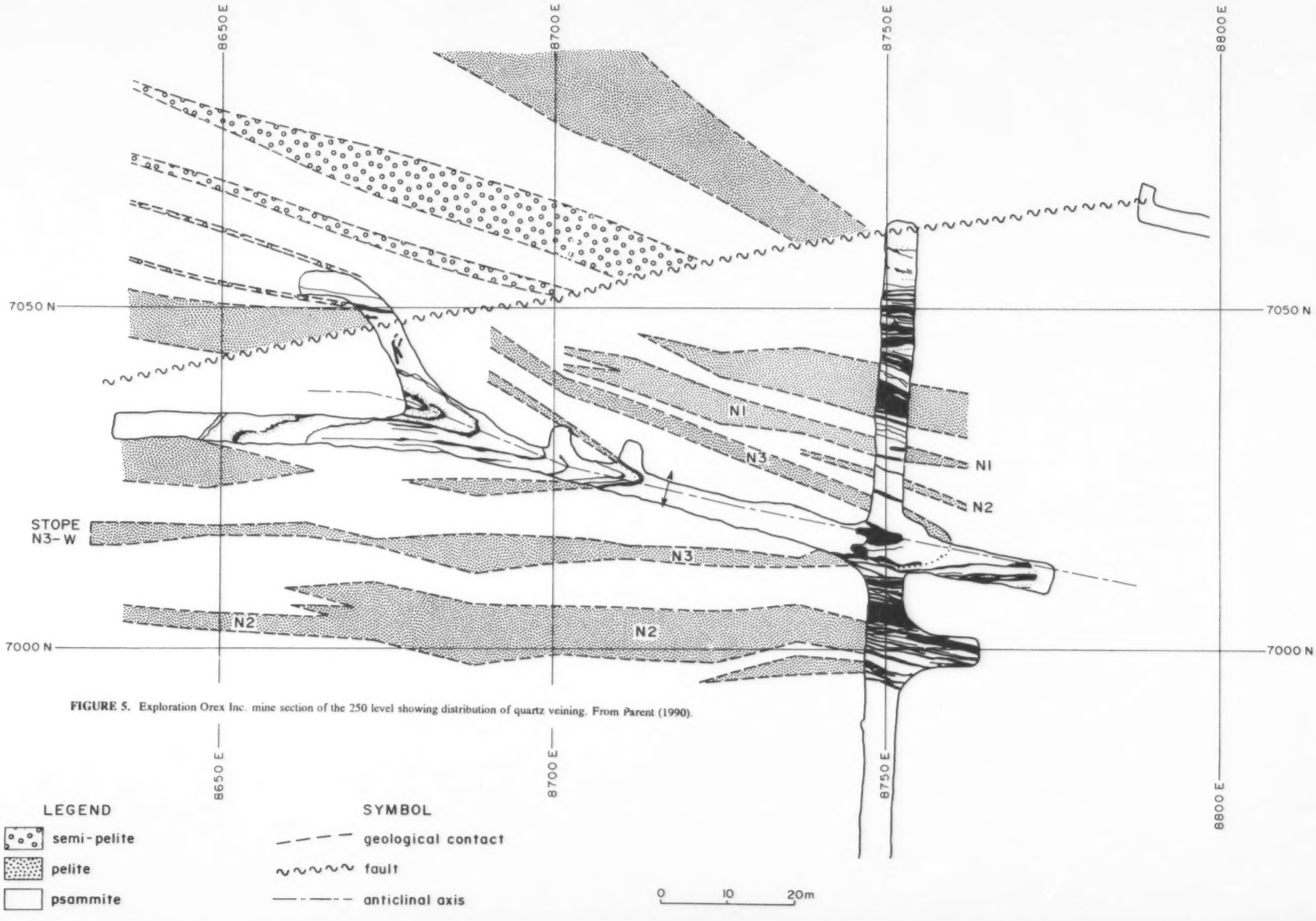

FIGURE 5. Exploration Orex Inc. mine section of the 250 level showing distribution of quartz veining. From Parent (1990).

most abundant auriferous veins, the most common type of auriferous quartz vein within the Boston-Richardson mine is the massive en echelon type.

A characteristic feature of most (all?) Meguma gold deposits is that the highest grades of gold occur within what appear to be structurally controlled ore-shoots. In this respect the Boston-Richardson mine is no different. The existence of gold-enriched ore-shoots were first noted in the original Boston-Richardson mine by Brown (1908), who mapped two ore-shoots, one on each limb within the Richardson belt on the 400 ft. level (Fig. 6). As shown in Figure 6 the oreshoots occur at a point of thickening within quartz-pelite belt, referred to by Brown (1908) as a roll. The ore-shoots appeared to plunge 25° to the east sympathetic with the plunge of the anticline but receede away from the fold axis with depth. The ore-shoot in the south limb was traced for 200 ft. along the level, while the shoot on the north limb was intersected 600 ft. from the fold axis and traced for 300 ft. along the level reaching a maximum thickness of 22 ft. The ore-shoots were traced from surface to the 700 ft. level (Malcolm, 1976). Recent work by Orex has indentified four similar ore-shoots, which appear to strike northwest and dip 45° to the northeast (P.K Smith, pers. comm.; Plate 3).

Prominent structural features within the mine area include a dextral(?) northwest-southeast trending fault which appears to have offset the Upper Seal Harbour anticline between the West Gold Brook and Boston-Richardson Mines (Fig. 3) and an approximately east-west (85°) trending shear zone which was intersected on the north limb of the anticline 18m from the fold-axis. The shear zone, which is indentified by a 2m wide fault breccia crosses the anticline at a shallow angle and appears to have caused minor dip-slip and dextral offset of the stratigraphy (Parent, 1990). Also present within the mine, are subvertical D_5 brittle-ductile shear and breccia zones (Plates 4a-c).

LITHOLOGICAL DESCRIPTIONS

Black pelite:

Within the Boston-Richarson mine the distribution of this facies appears restricted to the immediate area of the fold axis. As mentioned above, black pelite beds are the primary host for gold-bearing quartz veins. Recent, extensive surface and underground diamond drilling suggests that this facies is confined to a corridor $\leq$ 100 wide centered along the fold axis and that away from the fold axis grey pelite dominates. This observation implies that the black pelite may represent an alteration (carbonization?) facies characterized by graphite. Also indicated by diamond drilling is that the pelite beds are 2-3 times thicker at the fold axis compared to the limbs. The pelite is generally massive, has a well developed slaty cleavage (S_2) and may show evidence of a later crenulation cleavage (S_3; plate 5). The presence of chlorite and biotite (often retrograded to chlorite) indicates the effects of chlorite to biotite-grade, greenschist-facies metamorphism. Although no cordierite was seen in pelite samples during this study, it was reported in pelite from drill core in the vicinity of the Boston-Richardson mine. During this study, several pelite samples contained small orbicular biotite clots which may indicate alteration of cordierite porphyroblasts (see below). Also common within this facies are disseminated (<5-75%) fine-to coarse; <1mm -4cm) arsenopyrite, pyrite and pyrrhotite. In some instances, the appearance of arsenopyrite appears to be related to an alteration process particularly where it occurs in marked enrichment within wall rock adjacent to a quartz vein (Plate 6).

Psammite

This lithology is massive, medium -to locally fine-grained, and light to dark grey to green in colour. In the vicinity of the fold axis this facies is commonly interbedded/laminated with pelite and semi-pelite. It is characterized by a well developed pressure solution cleavage (S_2) which occurs as prominent brown stripes,

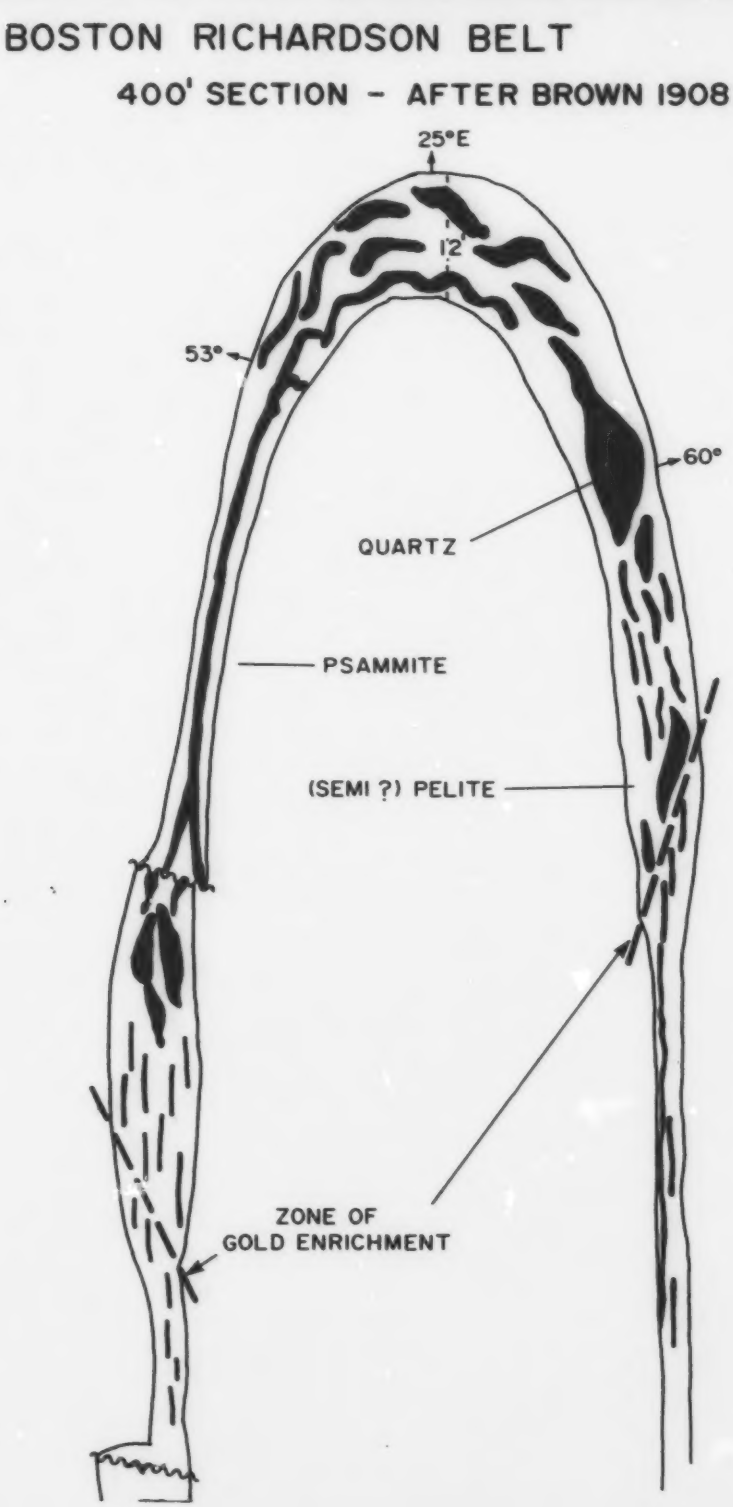

FIGURE 6. Distribution of quartz veining within the Boston-Richardson belt on the 400 ft. level as mapped by Brown (1908). The veins form an en echelon array of extension veins on both limbs. The fold hinge at this location plunges 25°E. Noted at the time were, the erratic distribution of quartz within the belt and an increase in coarse-grained quartz close to the fold axis. Also observed were zones of gold enrichment on both limbs associated with dramatic thickening of the belt. Recent work by Exploration Orex at the Boston-Richardson confirms Browns observations. The presence of en echelon veins in the area of the fold axis suggests that shearing post-dated folding.

referred to as 'tiger stripes' by Orex geologists. This facies contains carbonate oikocrysts and chlorite with minor biotite porphyroblasts and can host milky white quartz (AC?) veins (Plates 7a-c).

Semi-pelite

This lithology is typically biotite-rich (5-25%), dark-grey to black and shows a well developed crenulation cleavage. In addition to biotite this facies can contain abundant carbonate oikocrysts which may be crenulated in response to the S_3 cleavage and chlorite porphyroblasts. Within the deposit area this facies commonly occurs interbedded with pelite and psammite whereas away from the fold axis it occurs interbedded with psammite. En echelon quartz veins can occur within this facies at both locations (Plate 8a,b).

Alteration Facies

There is ample evidence of successive periods of alteration within the Boston-Richardson Mine. Alteration is manifested as; 1) bleached, silicified psammites and pelites within and adjacent to quartz veins, 2) carbonitized psammites and semi-pelites, soft and friable (fractured) graphite-rich pelites, 3) biotite $\pm$ sulphide enrichment in wall-rocks adjacent to quartz veins, and amphibolite-grade, calc-silicate pods within quartz veins which appear to be completely metasomatized wall rock fragments (Plates 9a-h). The mineralogy of several of these alteration-facies are further discussed below.

MINERALOGY AND MINERAL CHEMISTRY

The above lithologies are characterized by a mineral assemblage which includes variable modal amounts and textural varieties of; biotite + chlorite + tourmaline + plagioclase $\pm$ sphene $\pm$ calcite $\pm$ opaques (oxides + sulphides; see below) $\pm$ amphibole $\pm$ zircon. The above mineral assemblage is indicative of chlorite to biotite grade, upper Greenschist facies metamorphism. The presence of cordierite is inferred by the rare occurrence of pinite and also small blocky mineral grains characterized by a quartz interior rimmed by fine-grained biotite which may indicate retrograded cordierite (see below). Surprisingly, no garnet was seen in the samples collected for this study, although it was seen occuring with biotite-rich clots within some samples of calc-silicate alteration taken from the muck-piles. The occurrence of garnet, possible retrograde cordierite and amphibole as clots within altered wall rocks and quartz veins suggests that local, restricted zones of lower amphibolite-grade metamorphism (metasomatism?) did occur, possibly attributed to interaction with fluids related to quartz veining.

The textures and mineral chemistry of many of the accessory mineral phases are discussed below. Although the minerals selected occur within each of the facies described above, it is their occurrence within the quartz veins which was of particular interest due to their potential to characterize physio-chemical properties of the quartz veins.

The samples selected for petrographic and microprobe study are representative of the lithologic and metasomatic facies which occur within the Boston-Richardson deposit. Although the focus of the study was the Boston-Richardson mine, samples were also collected for comparative purposes from the other deposits along the Upper Seal Harbour anticline (Fig. 3).

The chemistry of the mineral phases were determined at Dalhousie University, Halifax using a JEOL 733 electron microprobe utilizing 4 wavelength spectrometers in conjuction with a LINK 131 eV EDS system and ZAP matrix correction program. The microprobe was operated at 15 Kv at approximately 12 na.

BIOTITE:

Biotite is a common mineral within all lithologies along the Upper Seal Harbour anticline in the area of the Boston-Richarson mine. Several texturally varieties occur including:
(1) ragged, irregular grains in groundmass oriented parallel to S_2. This biotite is pre-to syn S_2 and is commonly crenulated and contains wavy inclusion trails parallel to S_3 (Plate 10a). It is common to abundant in psammite and semi-pelite and less abundant within pelite; (2) post S_2, syn-to post-S_3 irregular grains and small euhedral laths. Post-S_3 biotite was not common, but overgrows the crenulation cleavage (and pre-S_3 biotite) or are oriented parallel to S_3 (Plate 10b). Both textural varieties show variable degrees of chloritization. Characteristic of semi-pelite, less common within pelite and rare within psammite lithologies; (3) $\leq$5mm grains within thin (<10mm) discordant quartz-calcite $\pm$ opaque (ilmenite, sulphides) angular veins. These veins show a range of formation from pre-S_2, as indicated by the presence of a penetrative S_2 cleavage, to post S_2 as indicated by biotite-filled en echelon veins formed as a result of the later crenulation cleavage (Plate 10 c,d). This biotite can be altered to chlorite; (4) coarse lenticular crystal aggregates ($\leq$15mm) fan-shaped clusters within and at the wall-rock contact with quartz veins (11 a,b). This type of biotite is commonly associated and/or intergrown with chlorite (after biotite?), ilmentite, rutile (small acicular needle aggregates within chloritized biotite) and less commonly with apatite and muscovite. The lenticular type of biotite may show some deformation (boudinaging). Coarse biotite also occurs associated with plagioclase, calcite, muscovite, chlorite, sphene and sulphides within granitoid pods present within some quartz veins (Plate 11c); (5) small grain clusters forming rims around a core containing quartz, sericite and chlorite. These aggregates are thought to represent altered (retrograde?) cordierite porphyroblasts (Plate 11d); (6) large subhedral laths mantling coarse-grained arsenopyrite euhedra and probably formed within pressure shadows developed during cleavage development (syn-post S_2).

Mineral chemistry:

Table 2 lists representative analyses of the textural types described above. Figure 7a shows the various textural types of biotite with respect to their Al^{iv} and Fe/(Fe+Mg) content. A noticeable (significant?) difference in Fe/(Fe+Mg) is shown between matrix biotite within semipelite and pelite samples and that which forms coarse clots and laths within the alteration facies and psammite. The latter-types are characterized by lower Fe/(Fe+Mg) contents (2.38-2.48) compared to the 2.52-2.6 range for the matrix biotites. The lower end of the matrix group (2.52-2.56) are from an intensely deformed (S_{3-4}?) black pelite. Al^{iv} contents for the two genetic types overlap with a range of 2.32-2.77. Figure 7b shows the biotites have a range of Ti content of .117-.278. This corresponds to a range in TiO_2 wt.% from 1.02 wt.% to 2.44 wt.%. This diagram indicates that biotite from within the alteration facies and quartz veins contain slightly more Ti (.229-.278) compared to biotite with the matrix of pelites and semi-pelites (Ti=.117-.187). Also shown on this diagram as an inset is the temperature diagram of LeBel(1979) which was calibrated based on the determined geothermometry of biotites within a porphyry copper deposit. As seen, the biotites from this study indicate a temperature of <300 to 430°C, with biotites from within the alteration facies and quartz veins reflecting the highest temperature. F content of the biotites is generally below detection level. However, coarse vein biotite from an deformed black graphitic pelite contained 0.648-0.678 wt.% F and vein biotite associated with chlorite and carbonate from a brecciated black graphitic pelite contained 1.04-1.2 wt.% F.

CHLORITE:

This mineral is also a common accessory phase in many of the rock types and alteration facies within the study area. Textural varieties observed include: 1) small (<2mm) to large (cm) irregular pale-green to deep brilliant-green grains (Plate 12a) within several of the alteration facies (calc-silicate pod, silicified psammite), these chlorite probably reflect replacement of biotite and plagioclase. This type also occurs within quartz and quartz-calcite veins where it may form lensoidal crystal clusters oriented normal to vein margins. This latter

TABLE 2. Representative microprobe analyses of biotite.

Sample	BB88-47-805	BB91-10	BB91-11	BB91-14	BB91-14	BB91-14	BB91-15	BB91-15	BB91-8	BB91-8
Analysis	3	4	1b	1a	2b	2c	4a	6b	3b	4
Location			*	*	*	*				
Mineral	BIO	BIO	BIO	BIO	BIO	BIO	BIO	BIO	BIO	BIO
SiO2	37.088	37.109	37.505	35.583	35.924	35.264	36.240	34.914	36.741	37.038
TiO2	2.444	2.093	1.198	1.057	1.177	1.140	1.624	1.472	1.185	1.191
Al203	17.388	18.015	16.323	18.649	18.939	19.300	18.510	17.185	17.411	17.165
FeO	17.065	16.752	15.723	20.527	20.059	20.020	19.297	19.822	16.286	16.811
MnO	.238	.656	.839	.267	.226	.182	.282	.334	.444	.407
MgO	11.750	12.013	13.048	8.943	9.025	8.693	9.988	9.243	11.781	12.061
CaO		-		-	.052	-	-	.052	-	-
Na20	.371	.358	.362	.271	.400	.398	.260	.294	.231	.380
K20	8.973	8.395	9.237	8.790	9.089	8.807	8.955	8.650	9.295	8.904
F	-	-	-	-	-	-	.678	-	-	-
Cl	-	-	-	.036	-	-	-	-	-	-
Total	95.32	95.39	94.24	94.12	94.89	93.80	95.83	91.88	93.37	93.96
Si	5.562	5.538	5.681	5.497	5.497	5.454	5.422	5.531	5.622	5.632
AlIV	2.438	2.462	2.319	2.503	2.503	2.546	2.578	2.469	2.378	2.368
AlVI	0.633	0.704	0.593	0.890	0.909	0.969	0.683	0.738	0.759	0.707
Ti	0.278	0.237	0.138	0.124	0.137	0.134	0.185	0.177	0.138	0.138
Fe	2.140	2.091	1.992	2.652	2.567	2.590	2.414	2.626	2.084	2.138
Mn	0.030	0.083	0.108	0.035	0.029	0.024	0.036	0.045	0.058	0.052
Mg	2.626	2.672	2.945	2.059	2.058	2.004	2.227	2.182	2.687	2.733
Ca	0.000	-	0.000	-	0.009	-	-	0.009	-	-
Na	0.108	0.104	0.106	0.081	0.119	0.119	0.075	0.063	0.069	0.112
K	1.717	1.598	1.785	1.732	1.774	1.738	1.709	1.748	1.814	1.728
CF	-	-	-	-	-	-	0.321	-	-	-
CCl	-	-	-	0.009	-	-	-	-	-	-
SUM CATS	15.532	15.488	15.667	15.574	15.602	15.578	15.330	15.589	15.608	15.608
Fe/(Fe+Mg)	0.45	0.44	0.40	0.56	0.56	0.56	0.52	0.55	0.44	0.44
Mg/(Fe+Mg)	0.55	0.56	0.60	0.44	0.44	0.44	0.48	0.45	0.56	0.56

Sample	DM12-12	DM12-12	DM12-12	RS-1	RS-1	WGB91-4	WGB91-4	WGB91-4	WGB91-4	WGB91-4
Analysis	5b	5ci	5cii	1	1i	3	5	5i	7	9
Location				PRE-S3	PPL-S3			INCL		
Mineral	BIO	BIO	BIO	BIO	BIO	BIO	BIO	BIO	BIO	BIO
SiO2	37.307	36.865	36.087	35.501	35.045	34.721	35.415	34.779	35.182	35.620
TiO2	2.313	2.053	2.207	1.620	1.418	1.186	1.188	1.089	1.152	1.142
Al2O3	17.479	17.756	17.530	18.722	18.994	18.435	17.518	17.840	18.212	18.357
FeO	17.343	17.148	17.090	20.598	20.132	21.044	20.348	20.410	20.707	20.970
MnO	.309	.131	.312	.370	.194	.143		.112	.294	-
MgO	11.274	11.344	10.992	8.930	8.786	8.739	9.237	9.231	9.353	8.752
CaO	.198	-	.164	-	-	.094	-	-	-	-
Na2O	.328	.360	.335	.278	.191	.358	.359	.249	.243	.312
K2O	9.031	9.045	9.244	8.929	8.663	8.864	8.360	8.590	7.979	9.089
F	-	1.206	1.085	-	-	-	-	-	-	-
Cl	-	-	-	.034	.029	-	-	.038	-	-
Total	95.58	95.91	95.05	94.98	93.45	93.58	92.42	92.34	93.12	94.24
Si	5.587	5.423	5.390	5.445	5.441	5.429	5.562	5.486	5.483	5.514
AlIV	2.413	2.577	2.610	2.555	2.559	2.571	2.438	2.514	2.517	2.486
AlVI	0.670	0.500	0.474	0.827	0.915	0.824	0.802	0.800	0.827	0.861
Ti	0.263	0.229	0.250	0.189	0.167	0.141	0.142	0.131	0.136	0.134
Fe	2.172	2.110	2.135	2.642	2.614	2.752	2.673	2.693	2.699	2.715
Mn	0.039	0.016	0.039	0.048	0.026	0.019	0.000	0.015	0.039	-
Mg	2.516	2.487	2.447	2.041	2.033	2.037	2.162	2.170	2.173	2.019
Ca	0.032	-	0.026	-	-	0.016	-	-	-	-
Na	0.095	0.103	0.097	0.083	0.058	0.109	0.109	0.076	0.073	0.094
K	1.726	1.698	1.761	1.747	1.716	1.768	1.675	1.729	1.587	1.795
CF	-	0.561	0.513	-	-	-	-	-	-	-
CCl	-	-	-	0.009	0.008	-	-	0.010	-	-
SUM CATS	15.514	15.143	15.230	15.576	15.529	15.666	15.563	15.613	15.534	15.618
Fe/(Fe+Mg)	0.46	0.46	0.47	0.56	0.56	0.57	0.55	0.55	0.55	0.57
Mg/(Fe+Mg)	0.54	0.54	0.53	0.44	0.44	0.43	0.45	0.45	0.45	0.43

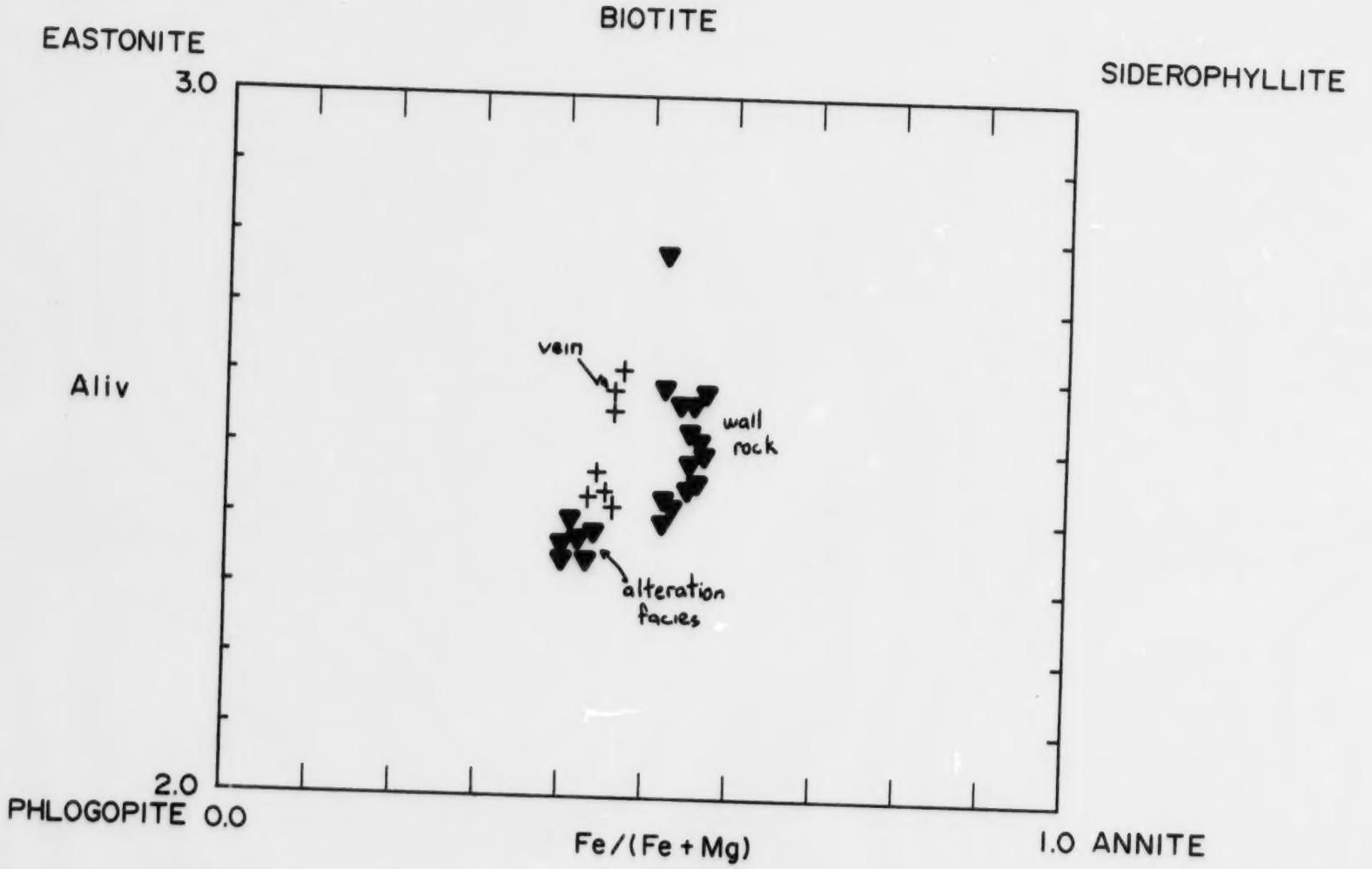

FIGURE 7a. Al^{iv} versus Fe/(Fe+Mg) binary classification diagram for vein, alteration facies and wall rock biotites.

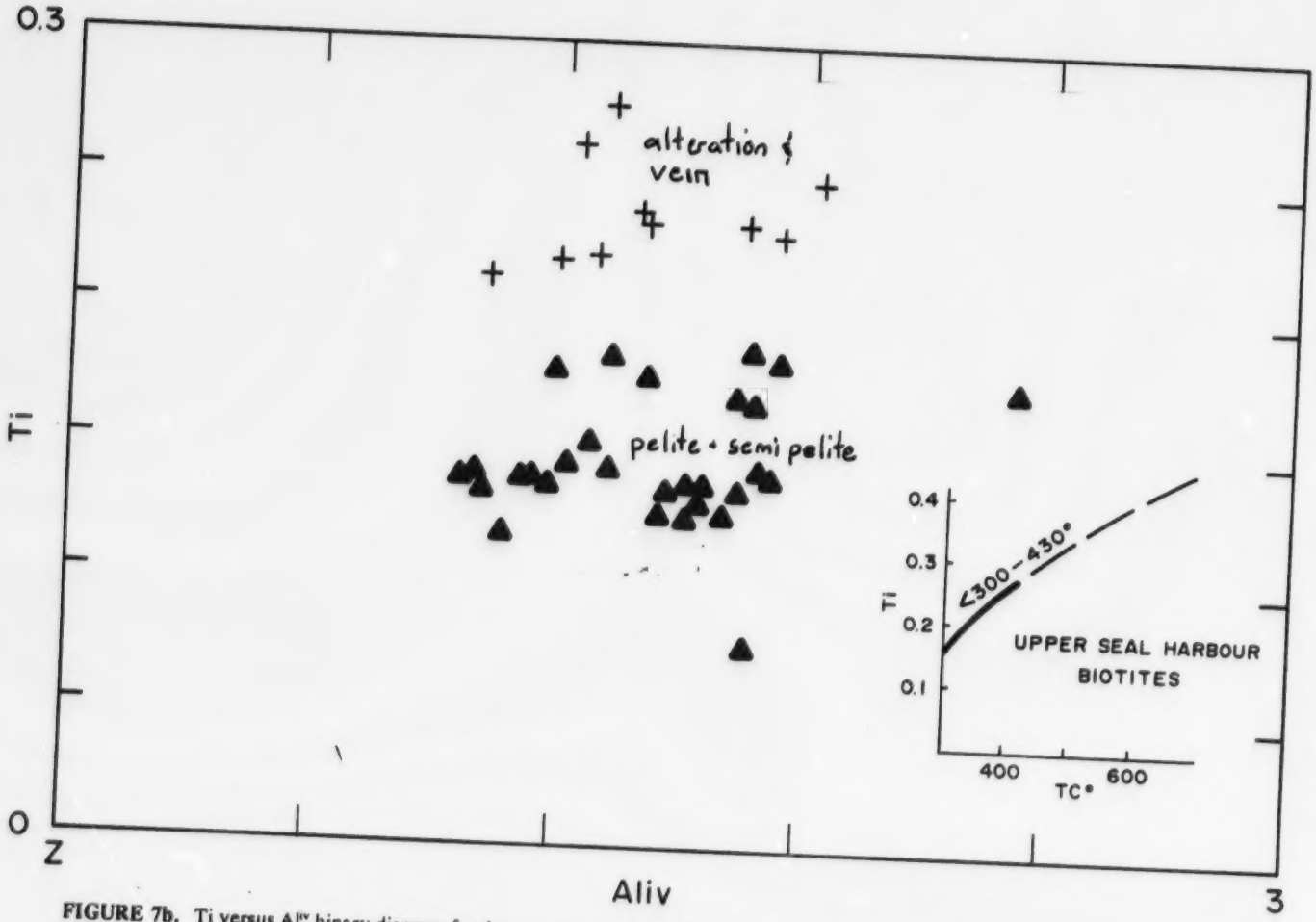

FIGURE 7b. Ti versus Al^{iv} binary diagram for the same group of biotites showing a slightly higher Ti concentration for biotites within the alteration facies and quartz veins compared to those within the matrix of pelites and semi-pelites. Inset is the biotite geothermometry diagram calibrated devised by LeBel (1979).

type shows increasing replacement of biotite from wall-rock contact into vein (Plate 12b); 2) large radial crystals and crystal masses associated with biotite + calcite ± muscovite ± sphene ± opaques within wall rock and quartz veins (Plate 12c). Much of this type of chlorite may be a result of biotite replacement as suggested by interlaminated biotite and the common presence of fine-grained rutile needles within the chlorite; 3) wormy aggregates within calcite and quartz veins (Plate 12d); 4) small, S_2-oriented, grains within the groundmass of pelite and psammite lithogies which are thought to reflect regional greenschist metamorphism.

Mineral chemistry:

Table 3 lists representative microprobe analysis of the various textural types of chlorite described above. Figure 8a shows that with the exception of two samples the chlorites plot within the ripidolite field as defined by Hey (1954). The two exceptions, which plot within Heys pychnoclore field, are pale-to dark-green chlorite grains hosting actinolite crystals (see plate 12a). The chlorite from this sample forms large silky, fibrous clusters within a quartz vein. These particular chlorites contain 21 wt.% MgO compared to 11.3 - 18 wt.% for the other chlorites, which is reflected by a Fe/(Fe+Mg) ratio of 0.32 compared to 0.41-0.57.

A difference between the chlorites is also shown in Figure 8b, which is a chlorite geothermometer devised by Jowett (1991) modifying the geothermometer of Cathelineau and Neiva (1985). As shown, the chlorites show a temperature range of 282-380°C. The lowest crystallization temperature are shown by the chlorites which host amphibole with estimated temperatures of 282.2 and 287.3°C. These are well separated from the rest of the chlorites which show a range of crystallization temperatures of 322.3-380.3. The highest temperatures are for large irregular chlorite grains occurring within quartz veins which appear to be replacements after biotite.

MUSCOVITE:

This mineral commonly occurs as small (< 1mm) grains showing a strong preferred S_2 orientation within the matrix of pelites and psammites (Plate 13). It also may be crenulated in response to the superimposed S_3 cleavage. Muscovite also occurs as large grains and fan-shaped crystal aggregates associated with chlorite ± biotite ± sphene within quartz veins and calc-silicate pods where it is associated with amphibole (see below). Some of the muscovite within the quartz veins appears to be a replacement of biotite as implied by the presence of pale brown biotite intergrown with the muscovite.

Mineral Chemistry:

Table 4 lists analyses of the muscovite described above. Their distribution according to Al^{iv} and Na/(Na+K+Ca) ratio is shown in Figure 9. The muscovite analyses which occur within the groundmass of a black, graphitic pelite are characterized by Na/(Na+K+Ca) ratios of ≤0.05 (i.e. paragonite component) and a low amount of biotite substitution (ΣFe+Mg+Mn+Ti=0.98, 1.17). Those which appear to be replacing biotite and are associated with biotite ± sphene ± amphibole are characterized by a higher concentration of Al^{iv} (1.15-2.08), biotite substitution (5.68-6.63) and slightly higher paragonite component (0.05-0.07). The dramatic increase in biotite substitution is matched by a decrease in Al^{vi} (phengitic component) from 5.49-4.64 for the groundmass muscovites to 2.27-0.35 for the amphibolite-grade muscovites. The single analysis of muscovite occurring within a chlorite + calcite-bearing quartz vein is characterized by low Al^{iv} (0.35) and biotite substitution (0.57) but a similar paragonite component (0.05). The above variations in biotite substitution are shown in Figure 9b which also shows the amount of celadonite (Si) substitution within the above muscovites. It is obvious from this plot that the analyses of muscovite coexisting with amphibolite are quite distinct from the groundmass muscovites. In fact, based on this diagram the former cluster at the phlogopite-annite end member. Based on experimental studies by Monier and Robert (1986) the muscovites reflect equilibration temperatures of 500-600°C for the groundmass muscovites and >800°C for the phlogopite end members. The

TABLE 3. Representative microprobe analyses of chlorite.

Sample	BR88-45-935	BR91-14	BR91-14	BR91-14	BR91-8	BR91-9	DM12-12	DM12-12	DM12-12	DM12-12
Analysis	1	1d	2	7	3a	2	1	3	5a	5c
Location	CHLOR	*	*	*				RADIAL		RADIAL
Mineral	CHL	CHL	CHL	CHL	CHL	CHL	CHL	CHL	CHL	CHL
SiO2	24.345	24.668	26.657	25.127	25.850	28.123	25.522	25.854	24.731	25.864
TiO2	-	.087	.102	.061	.129	-		.084	.082	-
Al2O3	20.286	21.173	20.492	20.698	20.882	18.527	21.575	20.674	20.839	21.400
FeO	26.620	27.068	19.407	25.945	21.189	17.239	23.051	22.813	22.948	22.981
MnO	.477	.444	1.233	.657	.618	.642	.630	.472	.458	.490
MgO	11.343	12.650	17.991	14.025	17.081	21.194	15.803	15.972	15.130	15.823
CaO	-	-	-	-	-	-	.084	.055	.039	-
Na2O	.218	.333	.338	.250	.298	.257	.097	.431	.355	.265
K2O	.070	.056	.673	-	.117	-	.032	-	-	.039
F	-	-	-	-	-	.548	.392	.563	.590	.441
Cl	-	-	-	-	-	-	-	-	-	-
Total	83.36	86.48	86.89	86.76	86.16	86.53	87.19	86.92	85.17	87.30
Si	5.480	5.349	5.547	5.398	5.447	5.798	5.383	5.478	5.370	5.442
AlIV	2.520	2.651	2.453	2.602	2.553	2.202	2.617	2.522	2.630	2.558
AlVI	2.858	2.756	2.570	2.634	2.629	2.297	2.741	2.637	2.699	2.746
Ti	-	0.014	0.016	0.010	0.021	-	0.000	0.014	0.014	-
Fe	5.011	4.908	3.378	4.661	3.734	2.973	4.066	4.042	4.167	4.044
Mn	0.091	0.082	0.217	0.120	0.110	0.112	0.113	0.085	0.084	0.087
Mg	3.805	4.088	5.580	4.490	5.364	6.512	4.967	5.043	4.896	4.962
Ca	-	-	-	-	-	-	0.019	0.012	0.009	-
Na	0.095	0.140	0.136	0.104	0.122	0.103	0.040	0.177	0.149	0.108
K	0.020	0.015	0.179	-	0.031	-	0.009	-	-	0.010
CF	-	-	-	-	-	-	-	-	-	-
CCl	-	-	-	-	-	-	-	-	-	-
SUM CATS	19.881	20.003	20.075	20.019	20.010	19.997	19.954	20.010	20.019	19.957
Fe/(Fe+Mg)	0.57	0.55	0.38	0.51	0.41	0.31	0.45	0.44	0.46	0.45
Mg/(Fe+Mg)	0.43	0.45	0.62	0.49	0.59	0.69	0.55	0.56	0.54	0.55

Sample	BB91-8	BB91-9	DM12-12	DM12-12
Analysis	3a	2	1	3
Location				RADIAL
Mineral	CHL	CHL	CHL	CHL
SiO2	25.850	28.123	25.522	25.854
TiO2	.129	-		.084
Al2O3	20.882	18.527	21.575	20.674
FeO	21.189	17.239	23.051	22.813
MnO	.618	.642	.630	.472
MgO	17.081	21.194	15.803	15.972
CaO	-	-	.084	.055
Na2O	.298	.257	.097	.431
K2O	.117	-	.032	-
F	-	.548	.392	.563
Cl	-	-	-	-
Total	86.16	86.53	87.19	86.92
Si	5.447	5.798	5.383	5.478
AlIV	2.553	2.202	2.617	2.522
AlVI	2.629	2.297	2.741	2.637
Ti	0.021	-	0.000	0.014
Fe	3.734	2.973	4.066	4.042
Mn	0.110	0.112	0.113	0.085
Mg	5.364	6.512	4.967	5.043
Ca	-	-	0.019	0.012
Na	0.122	0.103	0.040	0.177
K	0.031	-	0.009	-
CF	-	-	-	-
CCl	-	-	-	-
SUM CATS	20.010	19.997	19.954	20.010
Fe/(Fe+Mg)	0.41	0.31	0.45	0.44
Mg/(Fe+Mg)	0.59	0.69	0.55	0.56

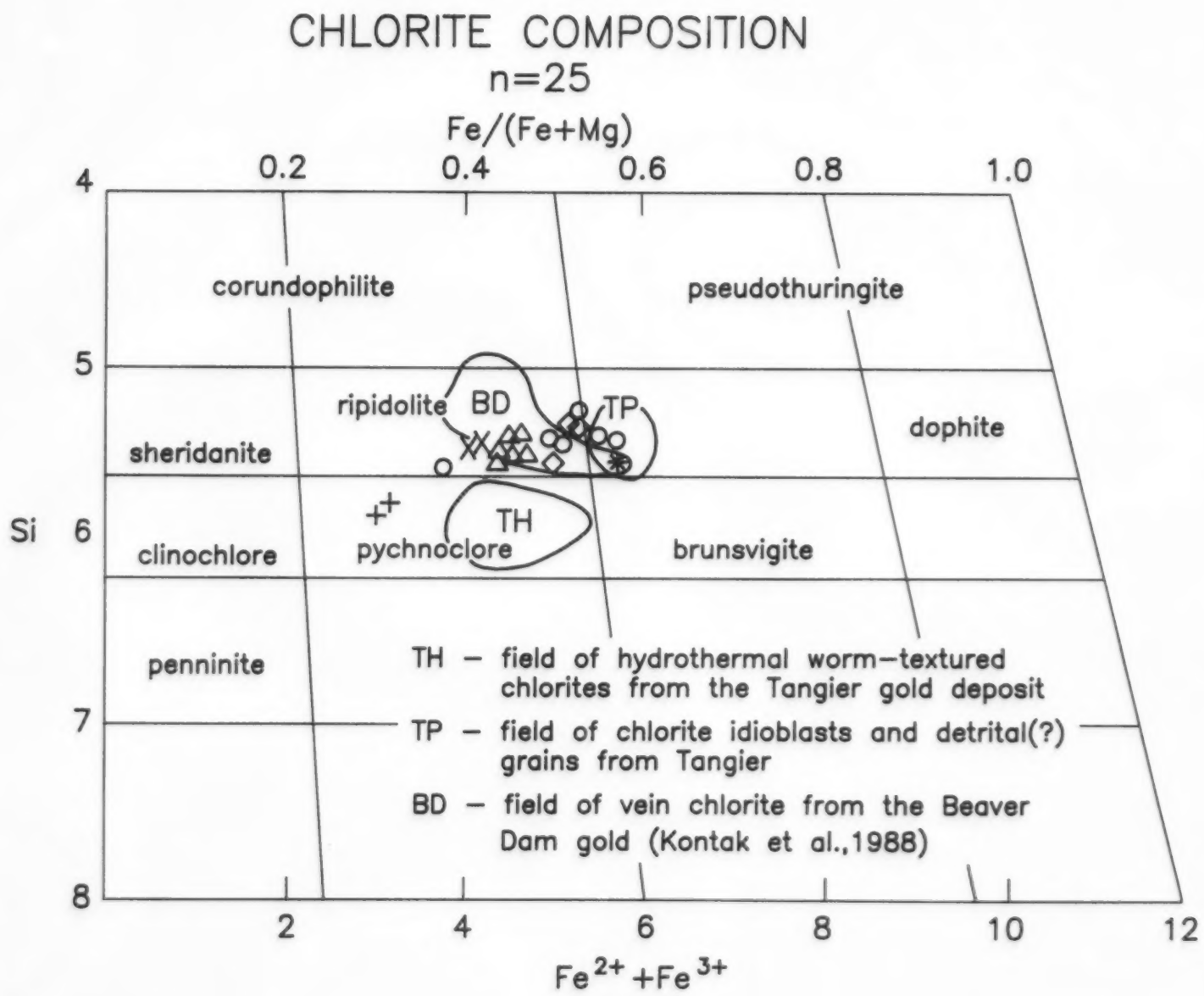

FIGURE 8a. Si versus $(Fe^{2+}+Fe^{3+})/(Fe^{2+}+Fe^{3+}+Mg)$ classification diagram of Hey (1984).

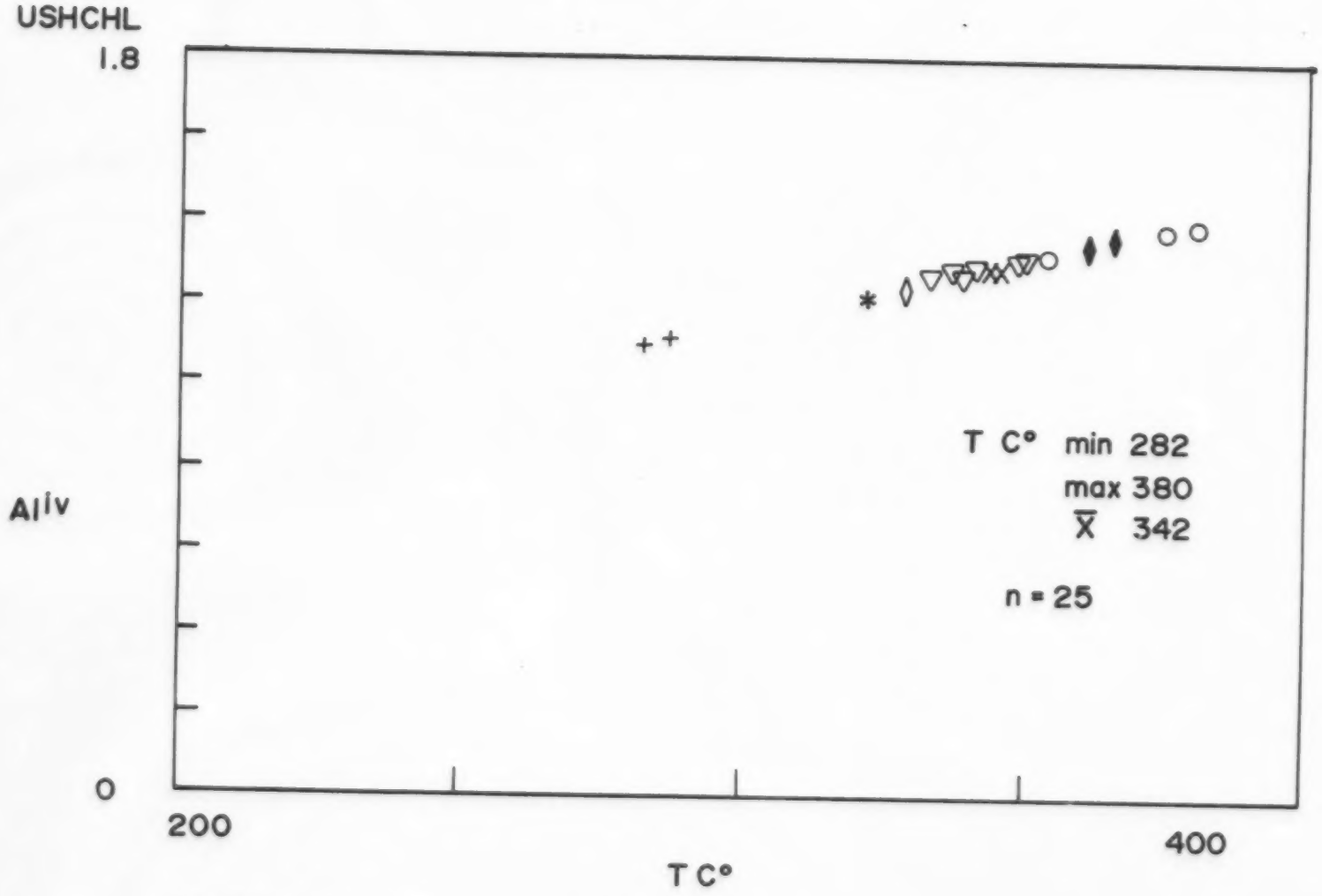

FIGURE 8b. Equilibration temperature estimates for chlorites based on the chlorite geothermometer after Jowett (1991).

TABLE 4. Representative microprobe analyses of muscovite and phlogopite.

Sample	BB88-47-805	BB91-13	BB91-14	BB91-9	BB91-9	BB91-9	DB91-6
Analysis	1a	5A	6f	1	11	2	1B
Location	*	MUSC	*	*	*	*	MUSC
Mineral	PHL	MUS	MUS	PHL	PHL	PHL	MUS
SiO2	40.285	46.145	47.466	38.334	38.966	38.969	46.860
TiO2	-	.179	-	.153	-	.159	.835
Al2O3	14.028	34.514	33.526	15.999	15.205	14.784	29.583
FeO	13.262	1.219	1.882	14.596	14.394	14.117	3.520
MnO	.244	-	.072	.341	.287	.393	.130
MgO	18.382	.812	1.282	16.327	16.974	17.242	2.590
CaO	.084	-	-	.054	-	.086	-
Na2O	.147	.354	.305	.399	.327	.274	.089
K2O	8.193	9.272	9.208	7.956	8.900	8.069	9.430
Cl	-	-	-	-	-	-	-
F	.084	-	-	1.325	1.380	1.429	-
Total	94.71	92.50	93.74	95.48	96.64	95.52	93.04
Si	5.922	7.013	7.653	6.385	6.560	6.577	7.251
AlIV	2.078	0.987	0.347	1.115	1.440	1.423	0.749
AlVI	0.350	5.190	6.018	2.269	1.575	1.515	4.643
Ti	-	0.021	-	0.021	-	0.020	0.098
Fe	1.630	0.155	0.254	2.192	2.056	1.993	0.456
Mn	0.030	-	0.010	0.052	0.040	0.056	0.017
Mg	4.027	0.184	0.308	4.370	4.259	4.337	0.597
Ca	0.013	-	-	0.010	-	0.016	-
Na	0.042	0.104	0.095	0.139	0.107	0.090	0.027
K	1.537	1.798	1.894	1.823	1.912	1.737	1.862
CCl	-	-	-	-	-	-	-
CF	0.039	-	-	0.753	0.735	0.763	-
SUM CATS	15.630	15.451	16.579	18.877	17.949	17.763	15.699
Fe/(Fe+Mg)	0.29	0.46	0.45	0.33	0.33	0.31	0.43
Mg/(Fe+Mg)	0.71	0.54	0.55	0.67	0.67	0.69	0.57
FM/(FMMTA)	0.94	0.06	0.09	0.74	0.80	0.80	0.18
Na/(Na+K+Ca)	0.03	0.05	0.05	0.07	0.05	0.05	0.01

PHL: phlogopite; MUS: muscovite

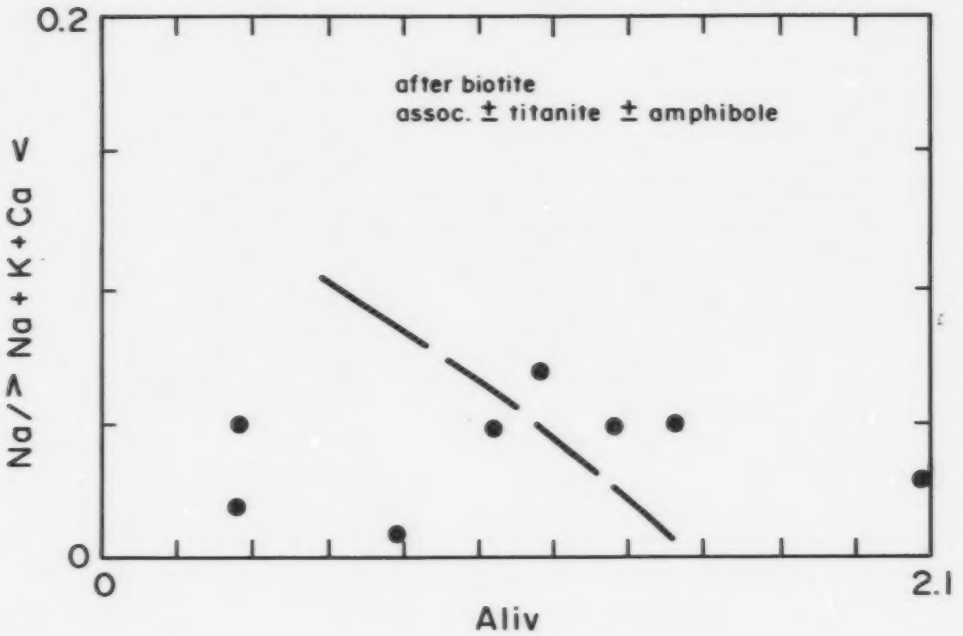

FIGURE 9a. Na/(Na+K+Ca) versus Al^{iv} binary diagram for muscovites.

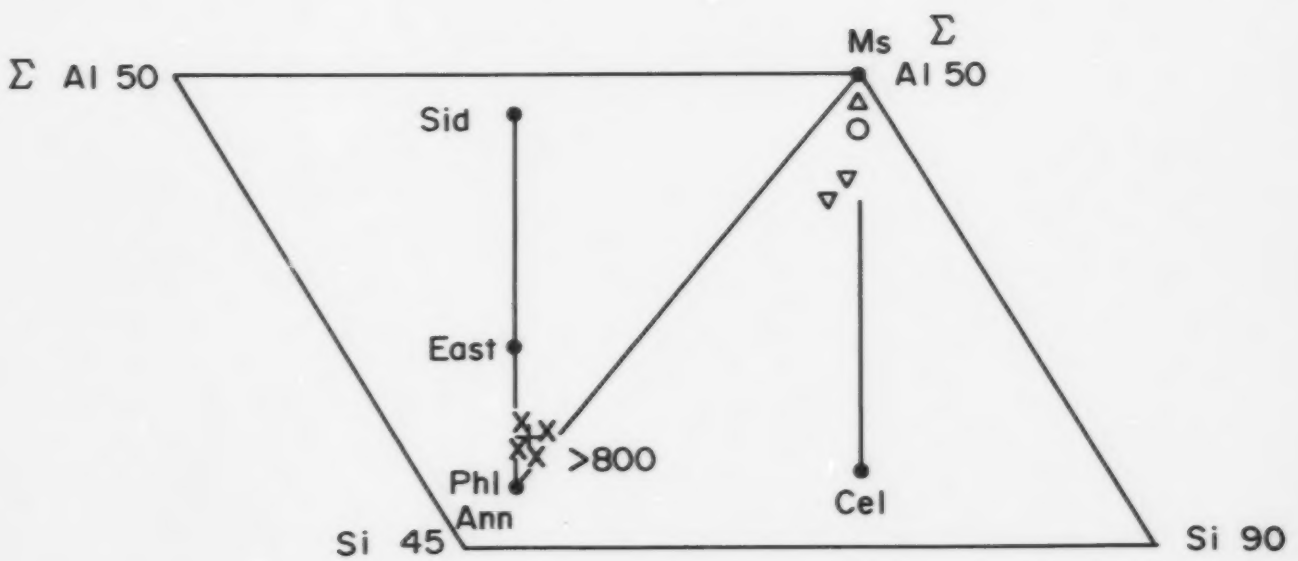

FIGURE 9b. Portion of Σ Al-Si-M^{2+} ternary diagram of Monier and Robert (1986) plotting muscovites from this study.

increased biotite substitution and decreased Al^{vi} within muscovite from amphibolite-grade rocks is consistent with the findings of Holdaway *et al.*(1988) who concluded that such behavior within muscovite reflects increasing metamorphic grade. The amphibolite grade muscovites are also distinct in that they contain minor F (1.32-1.65 wt.%).

PLAGIOCLASE:

The occurrences of plagioclase feldspar within the Boston-Richardson mine encompasses a wide variety of rock types and textures. As part of this study, plagioclase analysis were restricted to those occurring within quartz veins and altered rocks such as calc-silicate and pegmatitic pods. Plagioclase habits include; (1) small (< 1mm) well rounded and corroded grains (porphyroblasts?) within an intensely sericitized pelite, some of which show an unusual sector twinning (Plate 14a,b); (2) large (1-3mm) zoned grains with corroded cores associated with chlorite, calcite and rare scapolite (meionite) within quartz veins (Plate 14c; see Table 5); 3) unusual zoned plagioclase euhedra with intensely altered, black (graphitic?) cores which are surrounded by interstitial sulphides from within a calcite + chlorite + quartz vein (Plate 14d); and 4) relatively unaltered, polysynthetic-twinned grains within amphibole-bearing, calc- silicate pods.

Mineral Chemistry:

Table 5 lists the representative analyses of plagioclase described above from within quartz veins and the alteration facies. As indicated in Table 5 and shown in Figure 10 the composition of plagioclase within these rocks is quite variable ranging from An_{55} to $An_{<1}$. The potassium component of the plagioclase ranges from $Or_{<1}$ to Or_{43}.

Included as part of these analyses is a large oscillatory zoned plagioclase from within a chlorite + calcite-bearing quartz vein. This grain shows a transition from a core of An_{55} to a rim of virtually pure albite (Ab_{99}). The plagioclase grains containing the highest Or concentration (Or_{8-43}) occur as rounded corroded grains within a sericitic pelite and as grains containing abundant, small (< 0.5 mm) tourmaline needles (see below). The chemistry of these particular plagioclase grains is unusual within pelites (Kontak and Smith, 1987; in prep; Douma, in prep) and may reflect potassium metasomatism. The zoned plagioclase in plate 14d which co-exists with interstitial sulphides has a composition of An_{24}, similar to other plagioclase from within quartz veins.

TOURMALINE:

This mineral can vary from rare to abundant within the various rock types and alteration facies. Several textural varieties of tourmaline occur and include: 1) broken, euhedral and optically zoned grains (Plate 15a) within the matrix of psammite, pelite and semi-pelite associated with biotite + ilmenite ± muscovite ± chlorite and associated with chlorite and abundant sphene (Plate 15b) within a silicified psammite (?); this type of tourmaline was also rarely seen as an inclusion within arsenopyrite crystals; 2) very small acicular crystals as inclusions within a partially altered plagioclase from within a quartz + calcite + plagioclase vein (Plate 15c); and 4, long slender crystals and crystal clusters showing a prominent basal cleavage, overgrowing plagioclase within a brecciated and arsenopyrite-rich black, graphitic pelite (Plate 15d). This sample also contains abundant calcite and minor sphene.

Mineral chemistry:

Representative analyses of the above textural types of tourmaline are listed in Table 6. With the exception of tourmalines from a chlorite + sphene-rich silicified and carbonitized psammite the tourmalines have a fairly consistent composition intermediate between dravite and schorl. The exceptions show a transition from schorlitic

TABLE 5. Representative microprobe analyses of plagioclase.

Sample	BR91-11	BR91-11	BR91-11	BR91-11	BR91-14	BR91-14	BR91-14	BR91-14	BR91-14	BR91-14
Analysis	2c	3 (near)	4a	5b	1B	1B	1c	5a	5b	5c
Location		PLAG			PLAG	PLAG-C		CORE	CORE+1	CORE+2
Mineral	FEL	FEL	FEL	FEL	FEL	FEL	FEL	FEL	FEL	FEL
SiO2	62.355	59.360	59.622	60.982	59.150	58.834	58.262	53.869	54.506	55.103
Al2O3	25.048	26.394	25.065	24.488	24.796	25.092	25.989	29.244	28.847	28.316
CaO	1.485	6.133	6.943	5.931	7.313	7.455	7.867	11.640	11.110	10.6
Na2O	5.357	4.755	7.996	8.595	6.349	6.104	7.602	5.202	5.795	6.031
K2O	2.914	1.277	.149	.104	.045	.100	.089	-	-	-
Total	97.95	98.83	99.78	100.26	97.65	97.58	99.98	99.96	100.34	100.05
Ab	63.40	49.65	67.02	71.66	60.93	59.32	63.31	44.71	48.42	50.73
An	13.91	41.57	32.16	27.77	38.78	40.04	36.20	55.29	51.58	49.27
Or	22.69	8.77	0.82	0.57	0.28	0.64	0.49	0.00	0.00	0.00

Sample	BR91-14	BR91-14	BR91-14	BR91-14	BR91-15	BR91-15	BR91-15	BR91-16	BR91-8	DM91-7
Analysis	5d	5d	5e	5g	2c	2d	2ei	SCAPO.	6c	3
Location	CORE+3	RIM	RIM-1	RIM-1				2		PLAG
Mineral	FEL	FEL	FEL	FEL	FEL	FEL	FEL	UKN	FEL	FEL
SiO2	54.564	67.331	54.444	63.474	57.993	63.273	64.362	43.595	54.559	66.454
Al2O3	28.725	18.786	29.003	23.121	25.919	21.090	21.147	23.487	28.168	20.443
CaO	11.198	.107	11.388	4.499	5.927	2.103	2.041	26.697	10.757	1.594
Na2O	5.539	11.139	5.575	9.371	6.854	5.466	4.229	.072	5.838	8.892
K2O	-	-	-	.182	1.819	5.389	6.349	.037	.139	.108
Total	100.16	97.48	100.41	100.74	98.97	97.63	98.59	94.66	99.53	97.49
Ab	47.00	99.47	46.97	77.99	59.19	52.88	43.85	-	48.95	90.33
An	53.00	0.53	53.03	21.02	30.47	12.82	12.82	-	50.28	8.95
Or	0.00	0.00	0.00	1.00	10.34	34.30	43.32	-	0.77	0.72

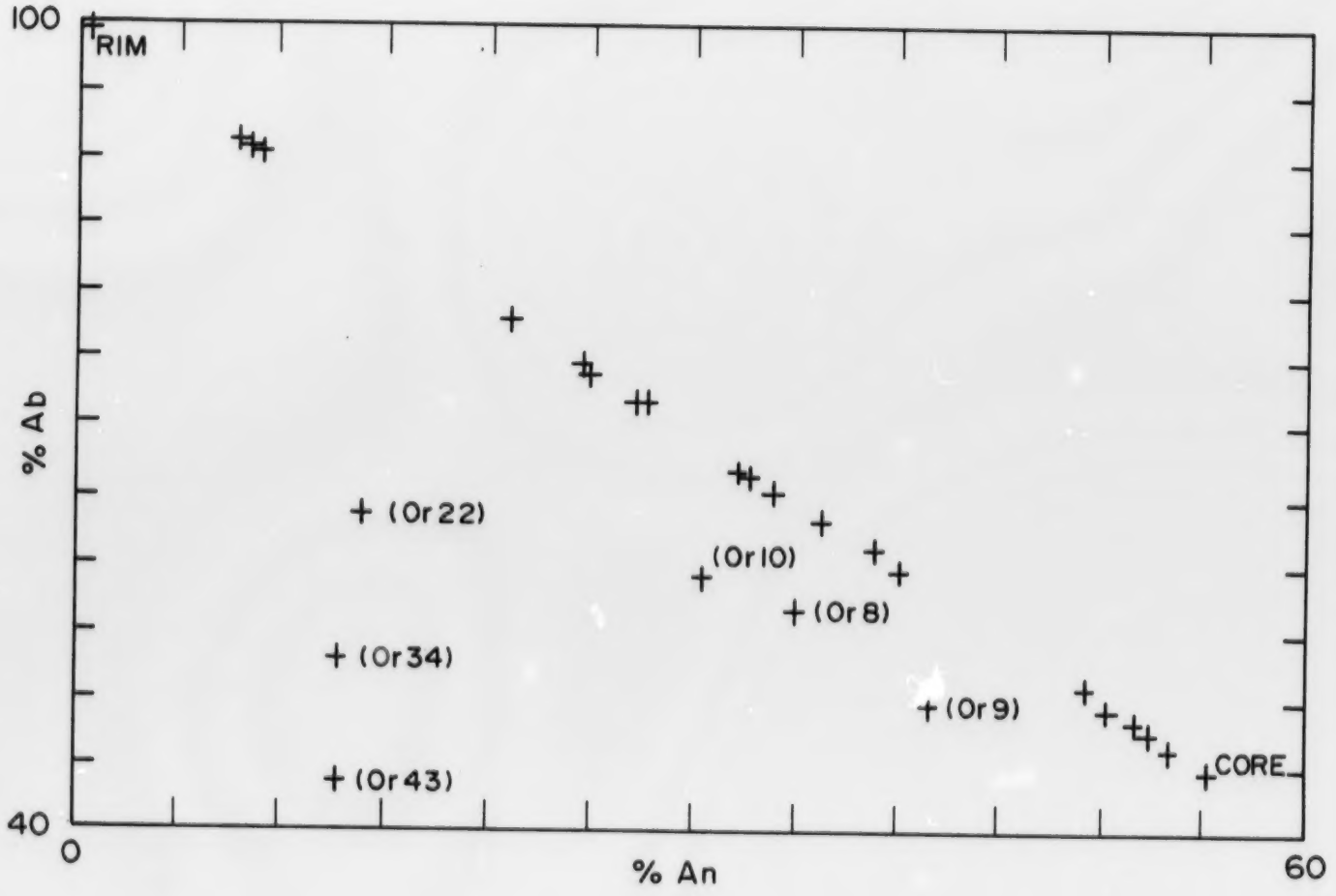

FIGURE 10. Ab versus An binary diagram for plagioclase feldspar analyses. Plagioclase which plot away from the regression line possess a higher Or concentration.

cores containing 10.2-10.4 wt.% FeO to rims of intermediate composition (Fig.11a). This compositional change is reflected by a distinct pleochroism characterized by blue-green cores and green-brown rims. The tourmalines show no significant concentration of MnO containing ≤ 0.38 wt.%. Figure 11b, which plots Fe/(Fe+Mg) over Na_2O wt.% shows the tourmalines contain only a minor elbaite component with Na_2O contents ranging from 1.5-2.15 wt.%. Fluorine concentration shows no textural correlation ranging from 0.81-1.2 wt.% within all of the tourmalines. With respect to the fields defined by Henry and Guidotti (1985) the tourmalines plot within the metasedimentary field with two samples bordering on the granitic field (Fig.11c). With respect to fields determined by Clarke *et al.* (1989) for granite-related barren and granite-related mineralized and nongranite mineralized (which includes tourmaline from Meguma gold deposits), the Upper Seal Harbour tourmalines overlap all three fields. This is similar to vein and wall rock tourmalines from Beaver Dam as shown by Kontak and Smith (in press).

APATITE:

Apatite is a common accessory mineral within quartz veins and the alteration facies where it occurs as coarse ≤ 1.5cm irregular grains associated with biotite ± calcite ± chlorite ± sphene ± muscovite and as small (< 1mm), irregular inclusions within calcite grains (Plate 16a,b). In quartz veins, apatite usually occurs adjacent to the wall rock contact associated with biotite clots which often show some degree of chloritization, particularly away from the contact. Apatite was also observed within quartz + chlorite +biotite-filled tension gashes in silicified psammite.

Mineral Chemistry:

Table 7 lists representative rim and core compositions for the types of apatites described above. The apatites are fluoroapatite, containing 2.74-3.45 wt.% F; and only trace MnO (<0.15 wt.%) and MgO (<0.12 wt.%). Figure 12 shows that the apatites have only slight compositional difference between core and rim. The composition of these apatites is comparable to those analysed from within the Beaver Dam gold deposit (Kontak and Smith, in press).

TITANITE:

Titanite is a common accessory mineral within quartz veins and altered wall rocks where it occurs as small(< 1mm) euhedral crystals and large(1-3mm), irregular grains associated with tourmaline and chlorite and, as small fracture-controlled grains (Plate 17a,b). This mineral also occurred as subhedral inclusions within saussuritized plagioclase from a granitoid segregation.

Mineral Chemistry:

Titanite analysis are listed in Table 8. The titanites are have variable TiO_2 and Al_2O_3 concentrations which range from 25.73 to 38.48 and 1.39-3.20 wt.% respectively. Although the majority of samples show no chemical distinction is possible, both analysis of titanite from a quartz vein hosted pegmatitic segregation contain significantly less TiO_2 than the other samples. Fluorine concentrations are ≤ 0.504 wt.% and FeO is ≤ .225 wt.%.

AMPHIBOLE:

Amphibole was indentified within three samples occurring as, radial clusters of small (<0.5 mm), fine-grained acicular crystals and larger broken and partially replaced crystals which may have a pale green colour but show no discernable pleochroism (see Plate 18). The samples are similar in that the amphibole occurs

TABLE 6. Representative microprobe analyses of tourmaline.

Sample	BB88-45-935	BB88-45-935	BB88-45-935	BB88-45-935	BB91-11	BB91-13	BB91-13	DM91-7	DM91-7	DM91-7
Analysis	1	1	1	1	2	2	2	1	1	2
Location	CORE	CORE2	RIM	RIM2	*	CORE	RIM	CORE	RIM	
Mineral	TOU	TOU	TOU	TOU	TOU	TOU	TOU	TOU	TOU	TOU
SiO2	34.761	35.162	35.669	36.097	37.028	34.080	36.277	36.648	35.262	36.966
TiO2	.203	.267	1.29	1.155	.186	.756	.688	.154	.999	.311
Al2O3	31.894	32.371	29.478	30.811	32.336	28.146	30.643	31.329	29.354	31.4
FeO	10.486	10.210	9.231	7.272	5.150	5.843	6.809	7.051	6.530	7.052
MnO	.384	.261	.105	.122	-	-	.076	.104	.088	-
MgO	3.217	3.439	5.589	6.213	7.225	6.310	6.511	6.191	6.562	6.587
CaO	.179	.277	.144	.955	.274	.093	-	.257	.685	.196
Na2O	1.824	1.760	1.998	1.609	1.528	1.873	2.150	1.770	2.034	1.875
Cl	-	-	-	-	-	-	-	-	-	-
F	.943	.932	.942	.924	.808	1.214	.987	.981	.843	.807
Sr	.093	.212	.135	-	-	-	-	-	-	-
Total	83.98	84.89	84.58	85.16	84.54	78.32	84.14	84.48	82.36	85.19
Si	7.247	7.236	7.353	7.293	7.364	7.519	7.398	7.430	7.341	7.387
AlIV	6.000	6.000	6.000	6.000	6.000	6.000	6.000	6.000	6.000	6.000
AlVI	1.831	1.846	1.157	1.331	1.574	1.313	1.359	1.481	1.197	1.390
Fe	1.828	1.757	1.591	1.229	0.857	1.078	1.161	1.196	1.137	1.179
Mg	1.000	1.055	1.717	1.871	2.141	2.075	1.979	1.871	2.036	1.962
Ti	0.032	0.042	0.202	0.177	0.028	0.127	0.107	0.024	0.158	0.047
Mn	0.068	0.045	0.018	0.021	-	-	0.013	0.018	0.016	-
Na	0.737	0.702	0.799	0.630	0.589	0.801	0.850	0.696	0.821	0.726
Ca	0.040	0.061	0.032	0.207	0.058	0.022	-	0.056	0.153	0.042
CF	0.622	0.607	0.614	0.590	0.508	0.847	0.637	0.629	0.555	0.510
CCl	-	-	-	-	-	-	-	-	-	-
Sr	-	-	-	-	-	-	-	-	-	-
SUM CATS	18.784	18.745	18.869	18.759	18.612	18.935	18.867	18.771	18.858	18.733
Fe/(Fe+Mg)	0.65	0.62	0.48	0.40	0.29	0.34	0.37	0.39	0.36	0.38
Mg/(Fe+Mg)	0.35	0.38	0.52	0.60	0.71	0.66	0.63	0.61	0.64	0.62

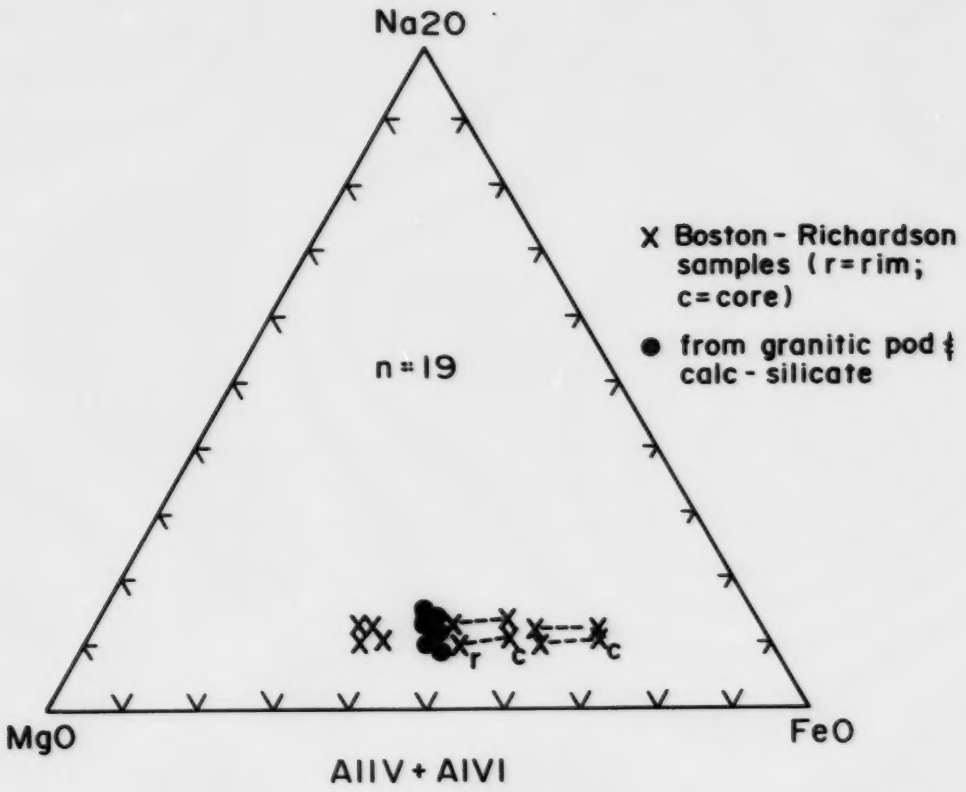

FIGURE 11a. Na_2O-MgO-FeO ternary plot for tourmalines showing their composition intermediate between dravite and schorl.

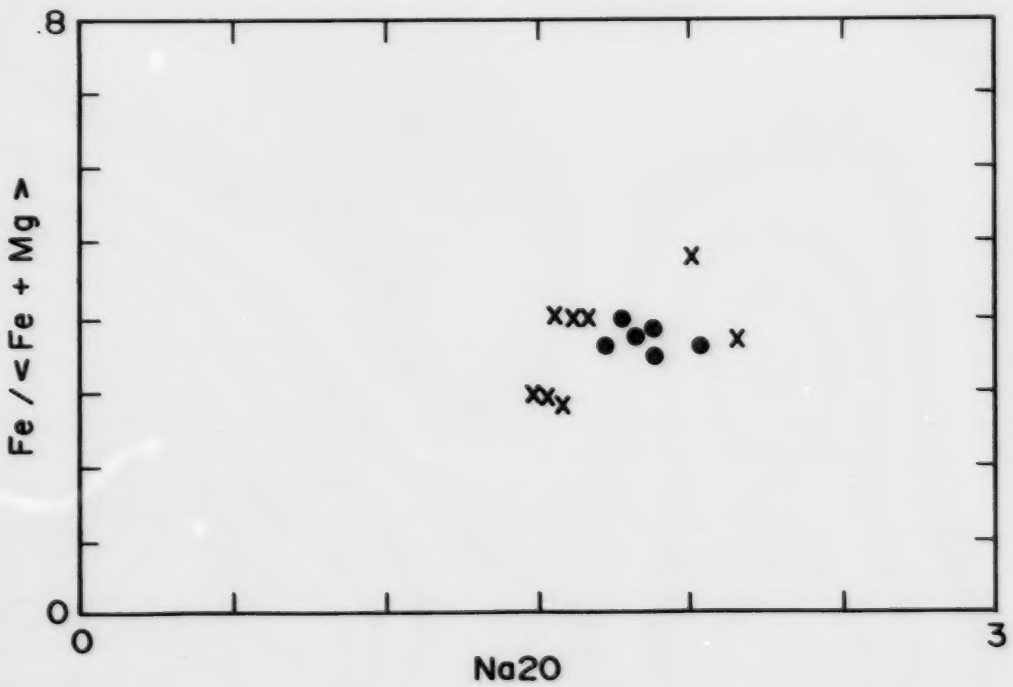

FIGURE 11b. Fe/(Fe+Mg) versus Na_2O wt.% binary diagram for tourmalines.

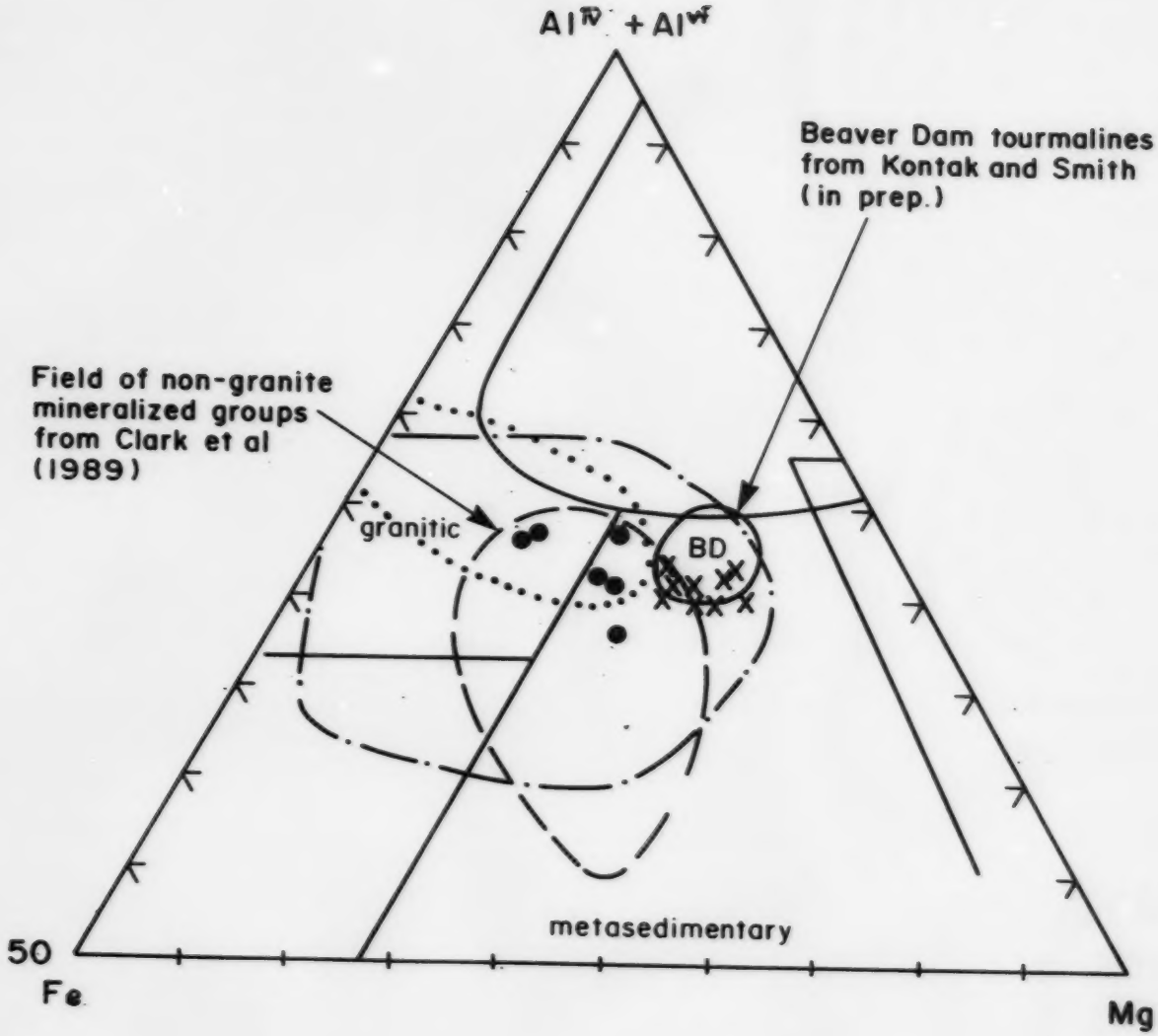

FIGURE 11c. Tourmalines plotted on ΣAl-Fe-Mg ternary diagram after Henry and Guidotti (1985).

TABLE 7. Representative microprobe analyses of apatite.

Sample	BR88-61-763	BR88-61-763	BR88-61-763	BR88-61-763	BR91-11	BR91-11	BR91-11	BR91-11	BR91-13	BR91-13
Analysis	*	*	*	*	TR-2	TR-2	TR-2B	TR-2B	TR-1	TR-1
Location	CORE	CORE2	RIM	RIM2	CORE	RIM	CORE	RIM	CORE	RIM
Mineral	APA	APA	APA	APA	APA	APA	APA	APA	APA	APA
FeO	-	-	-	-	-	-	-	.105	-	-
MnO	-	-	-	-	-	-	-	.150	-	-
MgO	-	-	-	-	-	-	-	.052	-	.053
CaO	54.362	54.131	54.672	53.853	54.634	54.585	55.065	55.603	54.163	54.881
Cl	-	-	-	-	-	-	-	-	-	-
F	3.360	3.315	3.347	3.187	3.314	3.435	2.785	2.853	3.290	3.202
P2O5	41.858	41.882	41.821	41.684	41.806	41.876	42.557	42.519	40.987	41.551
SrO	.254	.352	.339	.449	.251	.187	.430	.268	.428	.378
Total	57.72	57.45	58.02	57.04	57.95	58.02	57.85	58.76	57.45	58.14
P	-	-	-	-	-	-	-	-	-	-
Ca	18.606	18.632	18.633	18.729	18.659	18.554	19.142	19.025	18.655	18.747
CF	3.394	3.368	3.367	3.271	3.341	3.446	2.858	2.881	3.345	3.228
CCl	-	-	-	-	-	-	-	-	-	-
Mn	-	-	-	-	-	-	-	0.041	-	-
Fe	-	-	-	-	-	-	-	0.028	-	-
Mg	-	-	-	-	-	-	-	0.025	-	0.025
SUM CATS	18.606	18.632	18.633	18.729	18.659	18.554	19.142	19.119	18.655	18.772

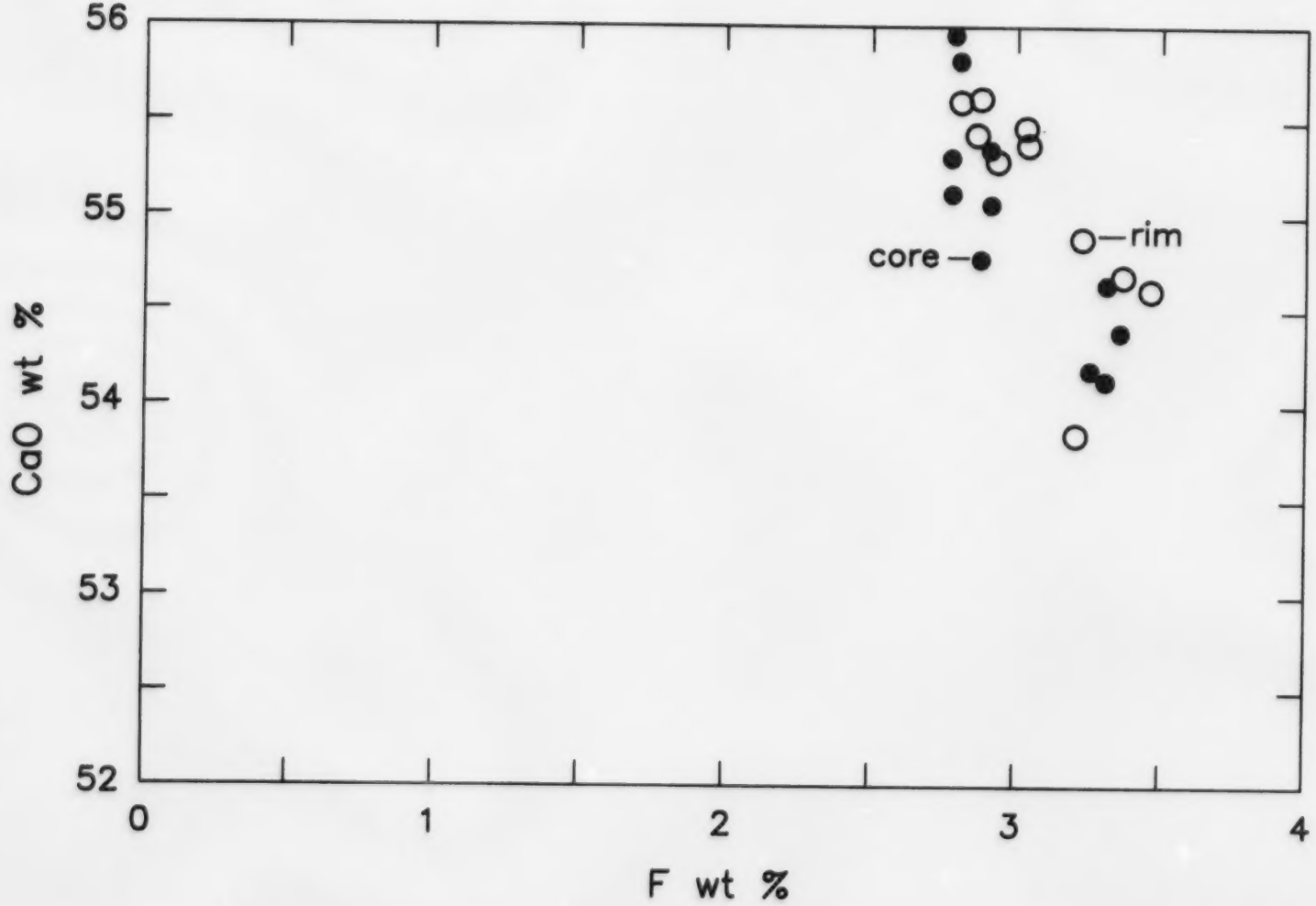

FIGURE 12. CaO wt.% versus F wt.% binary diagram showing rim-core compositions for apatites.

TABLE 8. Representative microprobe analyses of titanite.

Sample	BR88-935	BR88-935	BR88-935	BR91-15A	BR91-15A	BR91-8	DM12-12	DM91-6	DM91-6	WGB91-4
Analysis	1	1B2	3	1	2	6a	1	1B	3	7
Location	SPHENE	SPHENE	SPHENE	SPHENE	SPHENE	SPHENE	SPHENE	SPHENE	SPHENE	
Mineral	UNK	UNK	UNK	UNK	UNK	UKN	UKN	UNK	UNK	BIO
SiO2	30.522	30.821	30.525	30.503	30.463	30.124	30.760	30.344	30.518	35.182
TiO2	37.827	36.289	36.397	37.908	38.484	25.758	37.508	38.293	38.017	1.152
Al2O3	1.581	3.202	2.891	1.685	1.769	1.789	1.097	1.594	2.200	18.212
FeO	.160	.096	.225	-	-	.174	.088	-	-	20.707
MnO	.102	-	.	-	-	-		-	-	.294
MgO	-	-	.070	-	-	-	.080	.056	-	9.353
CaO	28.246	28.773	28.573	28.586	28.682	28.817	28.229	28.355	28.525	-
Na2O	-	-	.059	.067	-	.136	-	.122	-	.243
K2O	-	.043	-	.044	-	-	-	-	-	7.979
F	.249	.225	.204	.252	.190	-	.453		.183	-
Cl	-		-	.026	-	-	-	-	-	-
Total	98.69	99.45	98.94	99.07	99.59	86.80	98.21	98.76	99.44	93.12
Si	0.802	0.802	0.799	-	-	-	-	-	-	5.483
AlIV	-	-	-	-	-	-	-	-	-	2.517
AlVI	-	-	-	-	-	-	-	-	-	0.827
Ti	0.755	0.717	0.724	-	-	-	-	-	-	0.136
Fe	0.004	0.002	0.005	-	-	-	-	-	-	2.699
Mn	0.002	-	0.000	-	-	-	-	-	-	0.039
Mg	-	-	0.003	-	-	-	-	-	-	2.173
Ca	0.795	0.802	0.802	-	-	-	-	-	-	-
Na	-	-	0.003	-	-	-	-	-	-	0.073
K	-	0.001	-	-	-	-	-	-	-	1.587
CF	0.021	0.019	0.017	-	-	-	-	-	-	-
CCl	-	-	-	-	-	-	-	-	-	-
SUM CATS	2.38	2.423	2.425	-	-	-	-	-	-	15.534
Fe/(Fe+Mg)	1.00	1.00	0.64	-	-	-	-	-	-	0.55
Mg/(Fe+Mg)	0.00	0.00	0.36	-	-	-	-	-	-	0.45

associated with chlorite ± biotite ± calcite ± sphene within what appears to be intensely metasomatized wall rock fragments within a milky quartz vein (Plate 9e). The wall rock fragments have been completely replaced by the above amphibole-bearing assemblage and in some cases the accessory minerals appear to be replacements of amphibole. The similar mode of occurrence for amphibole within the samples suggests that this mineral is metasomatic in origin formed through interaction of wall rock with fluids attending quartz veining.

Mineral Chemistry:

The compositions of amphibole are listed in Table 9 and classified according to the Si and $Mg/(Mg+Fe^{2+})$ diagram of Leake (1978) in Figure 13. As shown the amphiboles have a fairly consistent composition and can be classified as actinolite, actinolitic hornblende and tremolite. The one exception is a Mg-Fe enriched sample classified as Mg-cummingtonite-gedrite although no textural dissimilarity was observed. These amphiboles have a similar mode of occurrence to the Al + Fe-enriched, ferro to tschermatic hornblendes indentified by Kontak and Smith (in press) from the Beaver Dam gold deposit.

CALCITE:

Calcite is a very common mineral within the Boston-Richardson samples where it shows a variety of habits ranging from; conspicuous large oikocrysts within the groundmass of pelites and psammites to large, coarse grains infilling vugs, fractures and shear/fault zones within quartz veins and wall rocks where it is commonly associated with chlorite + apatite + sphene + plagioclase. Calcite is also a common accessory mineral within quartz angular and en echelon quartz veins where it occurs as coarse, zoned grains.

Mineral Chemistry:

Calcite representing the above habits are listed in Table 10. The chemistry shows the calcites to have only minor Fe, Mg substitution. This is consistent with vein and wall rock carbonate from the Beaver Dam gold deposit analysed by Kontak et al (1988) and Kontak and Smith (in press) but contrasts with ferroan dolomite and ankerite carbonate indentified at other Meguma gold deposits (eg. Tangier, Cochrane Hill). An unusual, dark brown to orange carbonate was seen in a sample of black, highly graphitic, arsenopyrite-bearing pelite where it appears to occur as a pseudomorphic replacement of arsenopyrite (Plate 19). It addition to substantial FeO (35 wt %) and MnO (14 wt.%) this mineral contains minor SrO (2 wt.%), P_2O_5 (1.6 wt.%) and Na_2O_5 (1.7 wt.%).

SULPHIDES, OXIDES AND GOLD:

Figure 14 shows the paragenetic sequence for these minerals within quartz vein, wall rock and alteration facies specimens from the Boston-Richardson mine. The paragenesis of these minerals has been divided based on their relationship to the deformation features observed, specifically whether the mineral is orientated parallel to, overgrows or is deformed by a particular cleavage. Stage I represents minerals disseminated in wall and host rocks oriented parallel to S_2 cleavage. Stage II minerals are post-S_2, overgrowing the cleavage or occurring as inclusions within post-S_2 minerals, or conforming to S_{3-4} cleavages. These minerals commonly occur disseminated within quartz veins and alteration facies. Stage III minerals occur within S_{4-5} brittle-ductile structures. As shown in Table 1, these cleavages reflect deformation in response to specific events. The occurrence of abundant and paragentically long-lived arsenopyrite within the Boston-Richardson mine is consistent with virtually all other Meguma gold deposits. Within the Boston-Richardson mine this it occurs as fine- to- coarse-grained (< 1cm-4cm), euhedra disseminated within all rock-types. Within the psammite and pelite, arsenopyrite most frequently shows pre to syn S_2 development as indicated by the common presence of quartz-carbonate-chlorite-biotite filled pressure shadows (Plate 20a). Post- S_2 arsenopyrite occurring within these

TABLE 9. Representative microprobe analyses of amphibole.

Sample	BB88-47-805	BB91-9	BB91-9	BB91-9	BB91-9	BB91-9	BB91-9	BB91-9
Analysis	1a	1	2	2	2i	4	4i	5b
Location		s	CORE	RIM				
Mineral	AMP	AMP	AMP	AMP	AMP	AMP	AMP	AMP
SiO2	57.267	54.803	56.235	55.812	54.597	45.971	57.141	52.583
TiO2	-	-	-	-	.140		-	-
Al2O3	.313	2.463	1.031	1.935	2.506	4.898	.279	4.460
Cr2O3	-	-	-	-	-	-	-	-
FeO	8.953	9.842	8.098	8.939	8.688	15.876	7.913	10.903
MnO	.251	.814	.897	.772	.818	.851	.665	.984
MgO	19.421	17.380	18.785	18.301	18.025	16.557	19.884	15.985
CaO	12.037	12.362	12.553	12.714	12.237	7.432	12.128	12.078
Na2O	.091	.378	.282	.211	.423	.280	.227	.527
K2O	-	.081	-	.057	-	-	-	.138
F	-	.295	.245	.185	.137	.291	.249	.395
Cl	-	-	-	-	-	.035	-	-
Total	98.33	98.42	98.13	98.93	97.57	92.19	98.49	98.05
TSi	7.896	7.699	7.863	7.760	7.675	6.609	7.879	7.461
TAl	0.051	0.301	0.137	0.240	0.325	0.831	0.045	0.539
TFe3+	0.053	0.000	0.000	0.000	0.000	0.560	0.076	0.000
TTi	0.000	0.000	0.000	0.000	0.000	0.000	0.000	0.000
SUM IN T	8.000	8.000	8.000	8.000	8.000	8.000	8.000	8.000
CAl	0.000	0.108	0.033	0.077	0.090	0.000	0.000	0.208
CCr	0.000	0.000	0.000	0.000	0.000	0.000	0.000	0.000
CFe3+	0.522	0.353	0.267	0.307	0.404	1.349	0.477	0.489
CTi	0.000	0.000	0.000	0.000	0.015	0.000	0.000	0.000
CMg	3.991	3.639	3.914	3.792	3.776	3.548	4.086	3.380
CFe2+	0.457	0.803	0.680	0.732	0.618	0.000	0.359	0.805
CMn	0.029	0.097	0.106	0.091	0.097	0.104	0.078	0.118
CCa	0.000	0.000	0.000	0.000	0.000	0.000	0.000	0.000
SUM IN C	5.000	5.000	5.000	5.000	5.000	5.000	5.000	5.000
BMg	0.000	0.000	0.000	0.000	0.000	0.000	0.000	0.000
BFe2+	0.000	0.009	0.000	0.000	0.000	0.000	0.000	0.000
BMn	0.000	0.000	0.000	0.000	0.000	0.000	0.000	0.000
BCa	1.778	1.861	1.881	1.894	1.843	1.145	1.792	1.836
BNa	0.024	0.103	0.076	0.057	0.115	0.078	0.061	0.145
SUM IN B	1.803	1.964	1.957	1.951	1.958	1.223	1.852	1.981
ACa	0.000	0.000	0.000	0.000	0.000	0.000	0.000	0.000
ANa	0.000	0.000	0.000	0.000	0.000	0.000	0.000	0.000
AK	0.000	0.015	0.000	0.010	0.000	0.000	0.000	0.025
SUM IN A	0.000	0.015	0.000	0.010	0.000	0.000	0.000	0.025
CCl	0.000	0.000	0.000	0.000	0.000	0.009	0.000	0.000
CF	0.000	0.131	0.108	0.081	0.061	0.132	0.189	0.177
SUM CATS	14.803	14.978	14.957	14.961	14.958	14.223	14.852	15.006
SUM OXY	23.000	23.000	23.000	23.000	23.000	22.163	23.000	23.000
Group	-	2	-	-	-	-	-	-
Class	-	20	-	-	-	-	-	-
Name$	-	Actinolite	-	-	-	-	-	-
Type	-	-	-	-	-	-	-	-
Ca/K	-	-	-	-	-	-	-	-

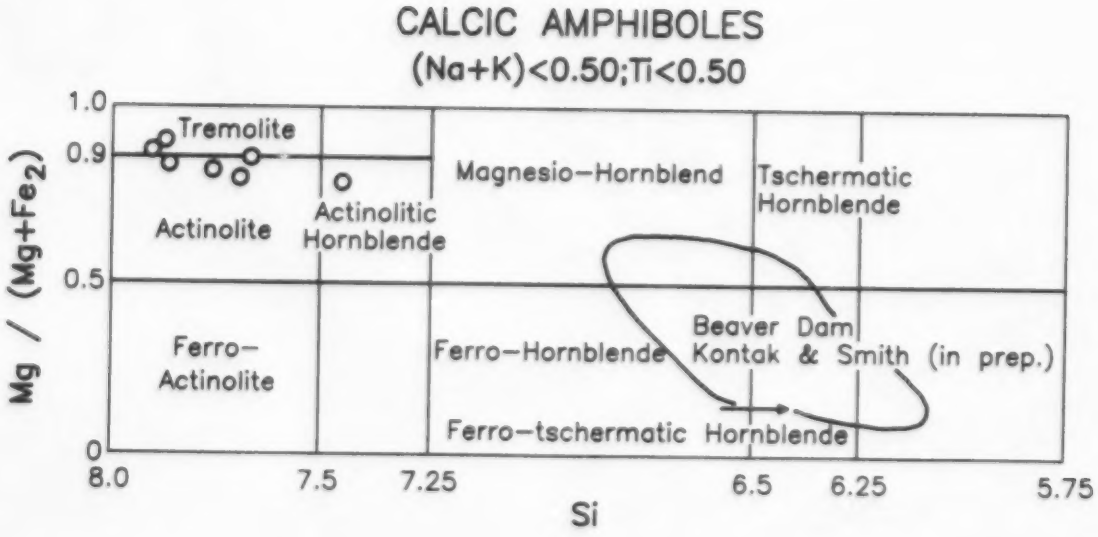

FIGURE 13. Si versus $Mg/(Mg+Fe^{2+})$ amphibole classification diagram after Leake (1978).

TABLE 10. Representative microprobe analyses of calcite.

Sample	BR88-45-935	BR88-45-935	BR91-11	BR91-11	BR91-11	BR91-11	BR91-11	BR91-11
Analysis	1	2	3	3B	3C	3D	6	7
Location	1	1	1	1	1	1	1	1
Mineral	1	1	1	1	1	1	1	1
SiO2	.141	.047	.091	.139	.105	.100	.053	.160
TiO2	-	-	-	-	-	-	-	-
Al2O3	-	-	-	-	.043		-	-
FeO	.379	-	.170	-	-	.595	-	-
MnO	.588	.623	1.299	1.910	.089	2.274	.114	1.346
MgO	.050	.103	-	-	-	.304	.041	-
CaO	55.483	56.124	56.968	57.201	56.640	55.645	55.484	54.866
Na2O	-	-	-	-	-	.053	.055	-
P2O5	.068	-	.106	.056	-	-	-	-
BaO	-	-	-	-	-	.197	-	-
Cl	-	-	-	-	-	-	-	-
F	-	-	-	-	-	-	-	-
Sr	.181	.049	.070	-	-	.094	-	-
Total	56.89	56.95	58.70	59.31	56.88	59.26	55.75	56.37

Sample	BR91-3	BR91-3	BR91-3	BR91-3	DR91-3	DR91-3	DR91-6	DR91-6
Analysis	4A	4B	4C	2	2B	2C	1A	1B
Location	1	1	1	1	1	1	1	1
Mineral	1	1	1	1	1	1	1	1
SiO2	.084	.105	.076	.133	.101	-	.669	.836
TiO2	-	-	-	-	-	-	-	-
Al2O3	-	-	-	-	-	-	-	-
FeO	.265	.874	.492	-	-	-	35.297	37.511
MnO	.783	1.033	1.050	8.274	4.254	9.680	-	-
MgO	.187	.376	.201	.298	.125	.390	14.114	16.764
CaO	56.015	55.972	55.900	53.445	55.772	51.126	.068	.135
Na2O	.126	-	.049	.077	-	-	1.691	2.031
P2O5	-	.094	-	.092	.063	.107	1.602	2.286
BaO	-	-	.135	-	-	-	-	-
Cl	-	-	-	-	-	-	.219	.186
F	-	-	-	-	-	-	.931	1.150
Sr	.128	.195	.104	.065	.153	-	2.052	2.973
Total	57.59	58.65	58.01	62.38	60.47	61.30	56.64	63.87

facies and quartz veins is normally coarse- to very coarse-grained euhedra overgrowing S_2. Arsenopyrite euhedra also commonly show intense brecciation in response to brittle D_5 deformation (Plate 20b). Marked modal enrichment of this mineral is also frequently seen within black, graphitic pelite wall rock adjacent to quartz veins (see Plates 5, 6). Arsenopyrite commonly contains inclusions of ilmenite and less commonly, pyrite, chalcopyrite, pyrrhotite, and rare sphalerite, galena, gold and Bi-tellurides (see below). Etching of the arsenopyrites reveals them to be compositionaly zoned (Plate 20b,c).

Galena occurs as small (< 1 mm), irregular inclusions within larger arsenopyrite euhedra and is often spatially associated with inclusions of gold, Fe±Ti-oxides, pyrrhotite, and rare Bi-Telluride and chalcopyrite inclusions. In some instances, galena grains contained discrete dark grey coloured bands which reflect increased Bi concentration (see below). Rare inclusions of gold were also observed within galena. Although pyrrhotite, pyrite and rarely chalcopyrite are present as inclusions within arsenopyrite these minerals most commonly occur as isolated grains and clusters within quartz veins and wall rock. This relationship together with the occurrence of these minerals as fracture-controlled stringers (in many cases en echelon) and interstitial, open-space infillings within S_{4-5} structures would suggest that they are paragenetically late and as such, show no relationship with gold.

Ilmentite habits include; irregular, rounded blebs within the lithofacies, minute inclusions within arsenopyrite and as coarse blades within quartz veins associated with sulphide minerals and rarely sphene. Rutile occurs as, fine-grained acicular needles within chlorite, representing exsolved Ti liberated through chloritization of biotite and as irregular, round grains associated with chlorite and calcite within brittle D_5 quartz-carbonate filled stringers (angulars). See plates 20d-h.

Gold within the Boston-Richardson mine occurs as micron-to rare millimetre sized disseminated grains within quartz veins, pelite and semi-pelite wall rock. The most common mode of occurrence was as irregular, micron-sized inclusions within arsenopyrite euhedra, where it is frequently associated with inclusions of galena and a Bi-telluride mineral (see below) in which gold also occurs as micron-sized inclusions. Gold is also present as fracture-fillings within fractured arsenopyrite euhedra, again associated with galena and rare Bi-telluride (Plate 21a-d). Such fractures in many cases represent brittle D_5 structures.

Mineral Chemistry

Sulphides: Tables 11 and 12 list the composition of the above minerals. Arsenopyrite analysis (Table 11a) which represent quartz vein and wall rock occurrences range in composition from 32-34.5 atomic % As and 31-33 atomic % Fe, similar to arsenopyrite from other meguma-hosted gold deposits (Kontak and Smith, in press). Such minor compositional variation is reflected by the zoned arsenopyrite euhedra which shows enrichment of Fe within core areas (Plate 21c). Three specimens of arsenopyrite contained significant concentrations of Ni (0.39-1.25 wt.%) and Pb (1.12 wt.%). The few analyses obtained of chalcopyrite and pyrrhotite show these phases to contain essentially no impurities, however, several analyses of paragenetically late pyrite (Table 11b) contain trace amounts (< 1.0 wt.%) of As, Zn, Ni and Au (0.26 wt.%). In contrast, analyses of galena inclusions and fracture-fillings (Table 12a) within arsenopyrite euhedra may contain significant Bi (≤6.5 wt.%) within discrete dark grey coloured bands (compare analyses EGB-4-2 and 2i), As (1.13 wt.%) and trace amounts of Te(≤0.58 wt.%), Ag(0.28 wt.%), Zn(0.27 wt.%) and Fe(0.25 wt.%). The Bi and Te-rich galenas are spatially associated with inclusions of gold within arsenopyrite. This association is not surprising since the gold analyses show that it also contains significant concentrations of Bi and Te.

Gold: As shown in Table 12b, gold is impure, containing considerable concentrations of Bi(27.12-31.51 wt.%) and Ag(1.52-1.76 wt.%) and trace Te(0.37-0.40 wt.%). The Bi-rich gold compound is very similar to a Bi-Au mineral indentified as maldonite (Au_2Bi) which was analysed from the tailings at the Lake Charlotte gold

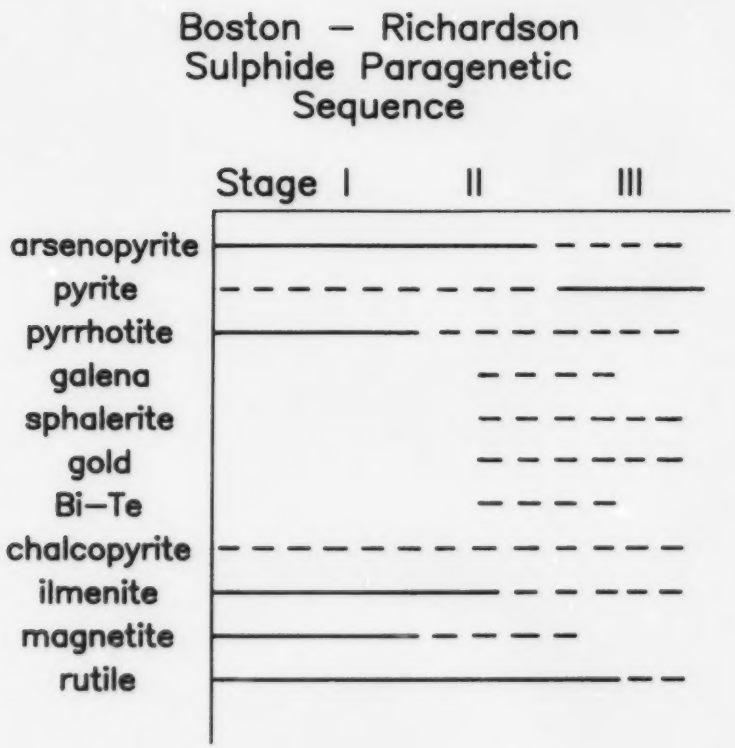

FIGURE 14. Sulphide-oxide-gold pargenetic sequence as determined from wall rock, alteration facies and quartz veins relative to the observed deformation features.

TABLE 11a. Representative microprobe analyses of arsenopyrite.

Sample	BB91-4	BB91-4	BB91-1	BB91-1	BB91-1	BB91-1
Analysis	1	5		2	3	3B
Location						
Mineral	ASP	ASP	ASP	ASP	ASP	ASP
Fe	34.579	33.913	33.459	33.027	33.425	33.406
Cu	-	-	-	-	-	-
As	45.381	47.875	45.894	45.236	44.333	45.574
Zn	-	-	-	-	-	-
Ni	-	.394	-	1.057	-	-
Pb	-	-	-	-	-	1.121
Ag	-	-	-	-	-	-
Au	-	-	-	-	-	-
Bi	-	-	-	-	-	-
Sb	-	-	-	-	-	-
Te	-	-	-	-	-	-
S	20.660	17.962	21.226	20.303	22.087	19.892
Total	100.62	100.14	99.78	99.62	99.84	99.99

TABLE 11b. Representative microprobe analyses of chalcopyrite and pyrite.

Sample	BB91-4	BB91-4	BB91-4	BB91-4	BB91-1
Analysis	10	10	5	5	3C
Location					
Mineral	CPY	PY	ASP	PY	PYR
Fe	30.208	46.204	33.913	45.655	59.690
Cu	34.959	-	-	-	-
As	-	.212	47.875	-	-
Zn	-	-	-	.219	.302
Ni	-	-	.394	.522	-
Pb	-	-	-	-	-
Ag	-	-	-	-	-
Au	-	.244	-	-	
Bi	-	-	-	-	
Sb	-	-	-	-	-
Te	-	-	-	-	-
S	35.321	52.941	17.962	53.874	40.973
Total	100.49	99.60	100.14	100.27	100.96

TABLE 12a. Representative microprobe analyses of galena.

Sample	BB91-4	DB91-1	DB91-1	DB91-1	DB91-1	BSB-4	BSB-4
Analysis	1	3B	3C	5	5ii	2	2i
Location							
Mineral	GAL	GAL	GAL	GAL	GAL	GAL	GAL
Fe	-		14.757	.254		-	-
Cu	-	-	-	-	-	-	-
As	-	-	17.961	-	-	-	1.131
Zn	-	-	-	.273	-	-	-
Ni	-	-	-	-	-	-	-
Pb	88.569	87.257	38.180	87.127	88.948	86.414	72.294
Ag	-	.281	-	-	-	-	-
Au	-	-	-	-	-	-	-
Bi	-	-	5.325	-	-	-	6.500
Sb	-	-	-	-	-	-	-
Te	.477	.582	.303	.392	.488	.595	.426
S	12.511	12.141	23.496	12.666	11.696	13.901	19.018
Total	101.56	100.26	100.02	100.71	101.05	100.91	99.37

TABLE 12b. Representative microprobe analyses of gold and tellurwismut.

Sample	DB91-1	DB91-1	DB91-1	DB91-1	BSB-4	BSB-4
Analysis	5	5ii	5ii	5iib	3	3i
Location						
Mineral	Au	Au	TEL	TEL	Au	Au
Fe	2.869	2.291	1.233	1.362	-	.689
Cu	-	-	-	-	-	-
As	1.642	1.250		-	-	-
Zn	-	-	-	-	-	-
Ni	-	-	-	-	-	-
Pb	-	-	.350	.300	-	-
Ag	1.540	1.527	-	-	1.766	1.594
Au	65.342	65.412	-	-	65.843	65.910
Bi	27.121	29.00	81.021	80.000	30.170	31.510
Sb	-	-	-	-	-	-
Te	.388	.373	16.595	17.246	.404	.398
S	.880	.672	-	-	-	-
Total	99.78	100.52	99.20	98.91	98.18	100.10

occurrence (Christovici & Leigh, 1982). Also, some gold inclusions within arsenopyrite (EGB-1a,b) contain only 22.33-42.58 wt.% Au with ≤9 wt.% Bi and trace Ag (≤0.89 wt.%) and Te (≤0.24 wt.%). These compositions are quite different from gold analysed from the Beaver Dam deposit by Kontak and Smith (in press) which contained significant Ag(3.42-44.26 wt.%) and much less Bi(≤5.10 wt.%). The existence of a Au-Bi-Te connection within the Boston-Richardson mine is further reflected by the occurrence of micron-sized inclusions of a Bi-Te mineral associated with gold and galena within arsenopyrite. This particular mineral has an average composition (n=5) of 80.5 wt.% Bi, 16.8 wt.% Te, 1.3 wt.% Fe, and trace Pb (0.32 wt.%). This composition is very similar to that of a Bi-Te mineral from the Beaver Dam deposit which has been tentatively indentified as Tellurwismut (Bi_2Te_3S) by Kontak and Smith (1988a). No wall-rock hosted disseminated gold was analysed in this study.

DISCUSSION

Aside from contributing to a growing data base for Meguma-hosted gold deposits, the results of this study allow for some interpretation regarding the nature of wall rock alteration, quartz veining and gold deposition along the Upper Seal Harbour anticline.

This study has revealed convincing macroscopic and microscopic evidence that successive periods of hydrothermal alteration occurred within gold deposits along the Upper Seal Harbour anticline and within the Boston-Richardson mine in particular.
Well defined macroscopic features such as silicified ± carbonitized psammites and pelites both as wall-rock and as fragments within quartz veins; the presence of black, graphitic pelite restricted to the area of the fold axis, and the erratic distribution of calc-silicate pods within wall-rocks and quartz veins indicates that significant interaction occurred between the host-rocks and fluids which presumably attended quartz veining. The fact that the distribution of black, graphitic pelite is coincident with extensive quartz veining within and proximal to the fold-axis is viewed as solid evidence of hydrothermal alteration. The black, graphitic pelite is not thought to represent a particular stratagraphic unit since does not occur on the limbs of the fold away from the the fold axis. The observed 3x thickening of stratigraphy associated with extensive quartz veining is curious and suggests that either dilation occured in response to a stuctural event unrelated to quartz veining (D_2-folding?) thereby creating a void into which the silica-rich fluids could collect, or alternatively, that dilation was induced by influx of a large volume of fluids. The abundance of massive, coarse-grained milky en echelon and sigmoidal quartz veins and lack of crack-seal textured quartz veins within the Boston-Richardson mine suggests that veining occurred synchronous with a period of active shearing that was likely syn- to-post D_2 deformation.

The calc-silicates are characterized by the assemblage, chlorite + titanite + calcite ± actinolite, tremolite ± muscovite ± apatite ± tourmaline ± scapolite (after plagioclase) ± phlogopite. The occurrence of calc-silicates within the quartz veins and wallrock may represent the metasomatic relacement of a pre-existing metamorphic mineral assemblage, perhaps reflecting local thermal doming in response to interaction with high temperature fluids attending quartz veining. Thermal doming has been invoked to explain the local occurrence of amphiboles within other Meguma-hosted gold deposits (Smith *et al.*, 1985). Application of the muscovite geothermometer of Monier and Robert (1986) indicates equilibration temperatures of 800°C for the phlogopites coexisting with actinolite. Muscovite as part of this assemblage equilibrated at 500-600°C. This occurrence of what appears to be a calcic-amphibole-bearing alteration assemblage may be analogous to similar alteration (actinolite + phlogopite + calcite + biotite) which occurs within some greenstone-hosted gold deposits and has been classified as skarn (Mueller & Groves, 1991). Accordingly, the actinolite + chlorite (after actinolite?) assemblage suggests that subsequent retrograde metamorphism (sub-amphibolite-facies) or alteration occurred. Figure 7b shows that chlorite associated with actinolite has a significantly lower equilibration temperature (282°C) compared to that for the other types of chlorite (322-380°C), correlating with a compostional range of pychnoclore to repidolite respectively. The highest equilibration temperature is for large grains of

presumably hydrothermal chlorites from within quartz veins. Pychnoclore chlorite has also been indentified from quartz-calcite veins hosted by chlorite-grade rocks within the Tangier deposit (Corey & Mills, in press).

Biotite analysed during this study show a wide range in texture, but show little compositional variation. The best discriminator is the Fe/(Fe+Mg) ratio which allows for differentiation between coarse-grained, alteration-facies and vein biotites and those occurring within matrix of wall rocks. Equilibration temperatures for the biotites range from a maximum of 430°C for quartz-vein biotite coexisting with calcic plagioclase to < 300°C for chloritized biotite from the matrix of wall rock. These temperatures are consistent with the range determined for vein and wall-rock biotites within the Beaver Dam gold deposit (Kontak & Smith, in prep).

The presence of zoned plagioclase with calcic cores (An_{55}) and albitic rims indicates high intitial temperatures (> 500°C) with subsequent equilibration below 400°C (Moody *et al.*, 1985). The presence of apatite + titanite + chlorite associated with altered plagioclase may reflect incorporation of Ca^{2+} released through albitization of calcic plagioclase and Ti^{4+} liberated through chloritization of biotite. The presence of scapolite ± chlorite after plagioclase may also indicate albitization. The occurrence of Or-rich plagioclase (Or_{8-43}) porphyroblasts within what appears to be a sericitized pelite is curious. Although the sericite-rich matrix suggests that the feldspars are a product of potassium-metasomatism, their prominent sector-twinning is unusual and if a primary feature, suggests rapid cooling of the plagioclase. The close textural similarity of these feldspars to cordierite may imply they represent pseudomorphic replacement of cordierite, except that no biotite is present as would be expected as a product from such a replacement reaction. The implied evidence of rapid cooling is consistent with evidence of rapid cooling inferred to have occurred within the Beaver Dam deposit based on zoning profiles within plagioclase and garnet (Kontak and Smith, in prep). Another unusual feature noted in plagioclase was the inclusion of abundant fine-grained tourmaline needles, which suggests that these phases likely co-crystallized.

The results of this study also allows for some speculation regarding the deposition of gold within the Boston-Richardson mine. Indicated, is a definite Au-Bi-Te-Pb-Ag association, manifested by significant concentrations of Bi (maldonite?), Ag and minor Te within the Au grains analysed and a strong spacial association with Bi-rich galena. Gold also occurs as micron-sized inclusions within a Bi-Te mineral which has been tentatively indentified as Tellurwismut, a mineral which has been indentified from within other Meguma-hosted gold deposits.

Since the gold analysed in this study occurs as micron-sized, inclusions within quartz vein hosted, large arsenopyrite euhedra, no comparison is possible with disseminated gold from within the wall rock. The presence of fracture-controlled gold, galena and possibly tellurwismut within arsenopyrite suggests that either the former were remobilized and redepositied within paragenetically later arsenopyrite or that a later period of gold deposition occurred. The fact that the arsenopyrite hosting such gold displays brittle deformation would require a syn- to-post D_4 timing (≤ 370 Ma.). A paragenetically late period of mineralization is also implied by $^{40}Ar/^{39}Ar$ geochronological studies by Kontak *et al.* (1990) which returned a plateau age of 366 Ma. from a sample of muscovite within a zone of massive quartz in on the 250 level of the Boston-Richardson mine.

CONCLUSIONS

This study has revealed mineralogy consistent with that determined from other Meguma-hosted gold deposits. The Boston-Richardson mine, which is hosted predominately by Upper Greenschist facies biotite-grade rocks, also shows the effects of Lower Amphibolite facies metamorphism reflected by the local occurrence of amphibole + biotite calc-silicate pods within and adjacent to quartz veins. The mineral chemistry indicates a range of equilibrium temperatures from > 500 to perhaps as high as 800°C to < 300°C, consistent with initial temperatures estimated from other Meguma-hosted gold deposits. Gold shows a definite association with

As+Bi+Te+Pb minerals, and its occurrence as inclusions in arsenopyrite, galena, tellurwismut and as < 1mm nuggets within wall-rock and fracture-infillings implies that two periods of gold mineralization may have occurred, the later possibly syn- to-post D_4.

ACKNOWLEDGEMENTS

The author would like to thank Dan Kontak and Paul Smith for sharing their extensive knowledge of Meguma-hosted gold deposits. Ron Mills is thanked for his assistance in the field. J. Campbell and colleagues are thanked for providing quality figures. The project was conceived by P. K. Smith and was funded by the 1990-92 Canada-Nova Scotia Mineral Development Agreement.

REFERENCES

Brown, E.P.,
1908: Notes on the geological structure at the Richardson mine as shown by plans and models of the same; in Trans. Min. Soc. Nova Scotia.13, p.17-26.

Cathelineau, M. and Nieva, D.,
1985: A chlorite solid solution geothermometer. The Los Azufres geothermal system (Mexico); Contrib. Mineral. Petrol. 91, 235-244.

Clarke, D.B., Reardon, N.C., Chatterjee, A.K., and Gregoire, D.C.,
1989: Tourmaline composition as a guide to mineral exploration: a reconnaissance study from Nova Scotia using discriminant function analysis; Eco. Geol. 84, p.1921-1935.

Christovici, M.A., and Leigh, G.W.,
1982: Recovery of gold from Lake Charlotte tailing (N.S.); Nova Scotia Department of Mines and Energy, Open File Report 587, p71.

Corey, M.C., and Mills, R.F.,
1992: Geological and geochemical observations within the Tangier gold deposit; Nova Scotia Dept. of Natural Resources Open File Report 92-008.

Douma, S.L.,
1988: Preliminary Report on the Metamorphic History of Meguma Group Metasediments in Eastern Nova Scotia; in Mines and Minerals Branch Report of Activities 1987, Part B; Nova Scotia Department of Mines and Energy. Report 87-5, p.121-129.

Douma, S.L.,
in prep: Structure and Metamorphic Evolution of the Eastern Meguma Terrane, Nova Scotia; Nova Scotia Dept Mines and Energy report in preparation. approx. 181 p.

Haynes, S.J.,
1983: Typomorphism of turbidite-hosted auriferous quartz veins, southern Guysborough County; in Mines and Minerals Branch Report of Activities 1983, Nova Scotia Department of Mines and Energy. Report 83-1, p.183-224.

Henry, D.J., and Guidotti, C.V.,
1985: Tourmaline as a petrogenetic indicator mineral: an example from the staurolite-grade metapelites of N.W. Maine; Amer. Mineral. 70, 1-15.

Hey, M.H.,
1954: A new review for the chlorites; Mineral. Mag. 13, p.277-292.

Holdaway, M. J., Dutrow, B. L. and Hinton, R. W.,
1988: Devonian and Carboniferous metamorphism in west-central Maine: the muscovite-almadine geobarometer and the staurolite problem revisited; Amer. Miner. 73, p.20-47.

Jowett, E.C.,
1991: Fitting iron and magnesium into the hydrothermal chlorite geothermometer. GAC-MAC Program Abstr. 16, A62.

Keppie, J.D.,
1983: Geological history of the Isaac's Harbour area, parts of 11F/3 and 11F/4, Guysborough County, Nova Scotia; in Mines and Minerals Branch Report of Activities 1983, Nova Scotia Department of Mines and Energy. Report 83-1, p.109-144.

Kontak, D.J. and Smith P.K.,
1988.a: Meguma Gold Studies IV: Chemistry of Vein Mineralogy; in Mines and Minerals Branch Report of Activities 1987, Part B; Nova Scotia Department of Mines and Energy. Report 87-5, p.85-101.

Kontak, D.J., Smith P.K., Kerrich R. and Williams, P.F.,
1990.a: An Integrated Model for Meguma Group Lode Gold Deposits, Nova Scotia, Canada; Geology, Vol. 18, 238-242.

Kontak, D.J., Smith P.K., Reynolds, P. and Taylor, T.,
1990.b: Geological and $^{40}Ar/^{39}Ar$ Geochronological Constraints on the Timing of Quartz Vein Formation in Meguma Group Lode Gold Deposits, Nova Scotia; Atlantic Geology, Vol. 26, 201-227.

Kontak, D.J., and Smith, P.K.,
in press: Geological and geochemical studies of a metaturbidite-hosted lode gold deposit: the Beaver Dam deposit, Nova Scotia: I. vein paragenesis and mineral chemistry.

LeBel, L.,
1979: Micas magmatiques et hydrothermaux dans l'environment du porphyre cuprifere de Cerro Verde-Santa Rosa; Perou. Bull. Mineral. 102, p.35-41.

Leake, B.E.,
1978: Nomenclature of amphiboles; Can. Mineral. 16, p.501-520.

Malcom, W.,
1976: Gold Fields of Nova Scotia. Geological Survey of Canada, Memoir 385, 253p.

Monier, G. and Robert, J.L.,
1986: Muscovite solid solutions in the system K_2O-MgO-FeO-Al_2O_3-SiO_2-H_2O: an experimental study at 2 kbar P_{H2O} and comparison with natural Li-free white micas; Mineral. Mag. 50, p.257-266.

Moody, J.B, Jenkins, J.E., and Meyer, D.,
1985: An experimental investigation of the albitization of plagioclase; Can. Mineral. 23, p.583-596.

Mueller, A.G. and Groves, D.L.,
1991: The classification of Western Australian greenstone-hosted gold deposits according to wallroc-alteration mineral assemblages; Ore Geol. Rev. 6, p.291-331.

O'Brien, B.H.,
1983: The structure of the Meguma Group between Gegogan Harbour and Country Harbour, Guysborough County; in Mines and Minerals Branch Report of Activities 1983, Nova Scotia Department of Mines and Energy. Report 83-1, p.145-182.

Parent, G., and Ethier, R.,
1989: Final report on the 1988 exploration program and ore reserve calculations on the Goldboro property, Guysborough County, Nova Scotia; Nova Scotia Department of Mines and Energy assessment report AR89-250; submitted by Exploration Orex Inc.

Parent, G.,
1990: Final report of the 1989-1990 exploration program and ore reserve calculations on the Goldboro property, Guysborough County, Nova Scotia; Nova Scotia Department of Mines and Energy assessment report AR90-15a; submitted by Exploration Orex Inc.

Smith, P.K.,
1983: Geology of the Cochrane Hill Gold Deposit, Guysborough Co., Nova Scotia; in Mines and Minerals Branch Report of Activities 1983; Nova Scotia Department of Mines and Energy, Report 83-1, p.225-256.

Smith, P.K., Haynes, S.J., and Reilly, B.A.,
1985: Turbidite-hosted gold deposits, Meguma domain, eastern Nova Scotia; Geological Association of Canada field guide, excursion II.

Smith, P.K. and Kontak, D.J.,
1987: Meguma Gold Studies: Some Basic Observations; in Mines and Minerals Branch Report of Activities 1986, Part A; Nova Scotia Department of Mines and Energy, Report 87-5, p.69-74.

Smith, P.K. and Kontak, D.J.,
1988.b: Meguma Gold Studies I: Generalized Geological Aspects of the Beaver Dam Gold Deposit, Eastern Meguma Zone, Nova Scotia; in Mines and Minerals Branch Report of Activities 1987, Part B; Nova Scotia Department of Mines and Energy. Report 87-5, p.45-61.

Williams, P.F. and Hy, C.,
1990: Origin and Deformation and Metamorphic History of Gold Bearing Quartz Veins on the Eastern Shore of Nova Scotia; in Mineral Deposit Studies in Nova Scotia, Vol 1.,Geol. Surv. Can. paper 90-8, p.169-195.

PLATES

1a. Specimen of folded, crack-seal textured, arsenopyrite-bearing quartz vein from within the Boston-Richarson mine. Quartz veins of this type are not common within the Boston-Richardson mine in contrast to most Meguma-hosted gold deposits.

1b. Photo showing typical en echelon quartz vein array within semi-pelite beds proximal to the fold axis. The veins appear to be right-stepping towards the fold axis. The proportion of quartz veining within the beds can vary from 0% to almost 100% within pelite beds at the fold hinge (see Fig. 4).

1c. Example of massive milky-white quartz vein containing a black, graphitic pelite lense which also shows the effects of probable D_3 shearing.

1d. Specimen showing massive AC vein cross-cutting earlier, S_2-transposed quartz vein, suggesting multistage quartz veining occurred.

2. A section of a quartz-pelite belt at the fold axis within the Boston-Richardson as exposed on the 250 level of the Exploration Orex Inc. development. The plate shows the prevalence of en echelon and oblique shear veins within the belts.

1a
cm

1b

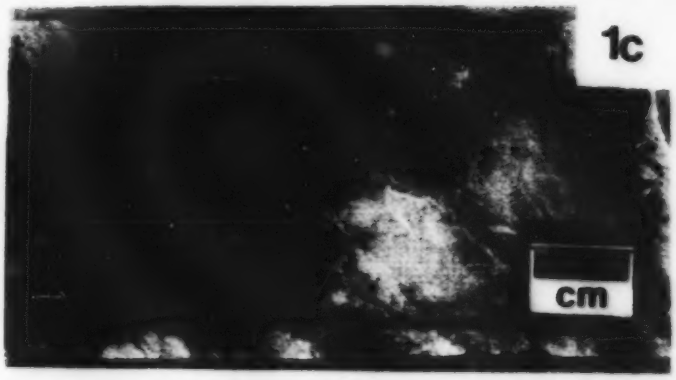
1c
cm

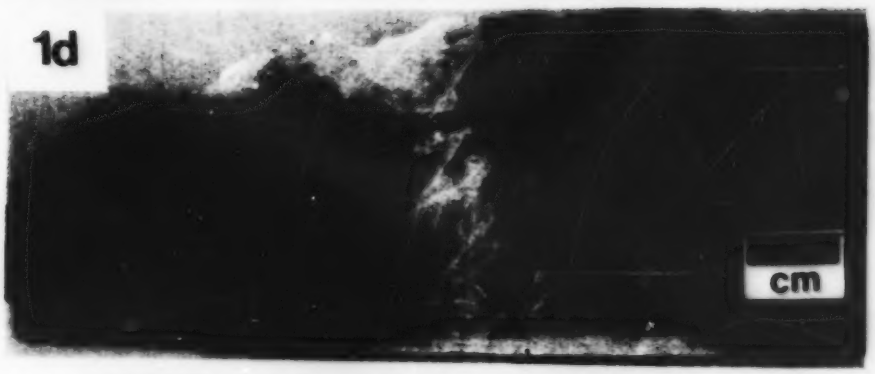
1d
cm

2

3. Drill core specimens of psammite showing kinked pressure solution stripes. This particular kink plunges 40° south, similar in orientation to that determined by Brown (1908) for a gold-enriched ore-shoot within the Boston-Richardson belt as exposed at the time on the 400 ft. level. Detailed mapping at the fold axis northwest of the Dolliver Mountain prospect also indentified sinistral kink-banding striking 148° with a 40° plunge to the south.

4a. Sample of drill-core from the Boston-Richardson mine showing presence of D_5 fault gouge adjacent to massive quartz vein.

4b. Calcite-filled, brittle D_5 shear zone in semi-pelite.

4c. Brittle-ductile D_5 shear zone within intensely chloritized psammite.

5. Arsenopyrite-rich, black graphitic pelite containing abundant brown, quartz-carbonate oikocrysts. The oikocrysts show the effects of D_2 and D_3 deformation and the absence of pressure shadows around the arsenopyrite indicates that it is post-S_2 in origin. Pelite such as this can contain gold as disseminated, micron-sized grains or as inclusions within arsenopyrite associated with galena.

6. Plate shows zone of hydrothermal enrichment of arsenopyrite along bedding contact of semi-pelite and black, graphitic pelite. The latter is host to a massive quartz vein.

7. Prominent S_2 pressure solution cleavage within psammite from adjacent to the fold axis.

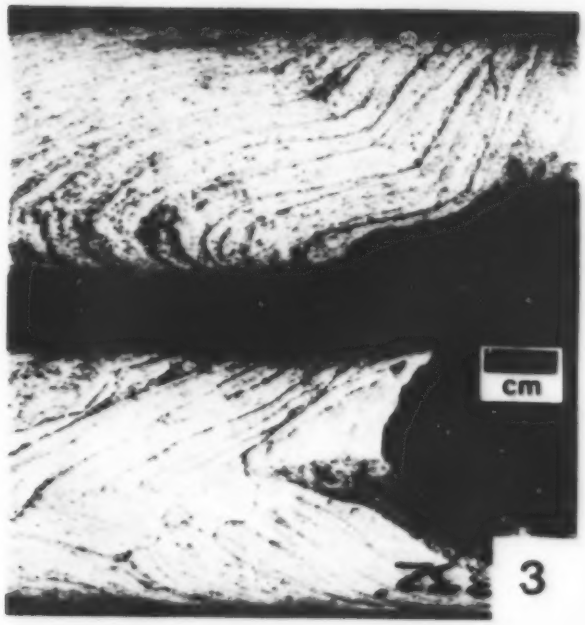

3

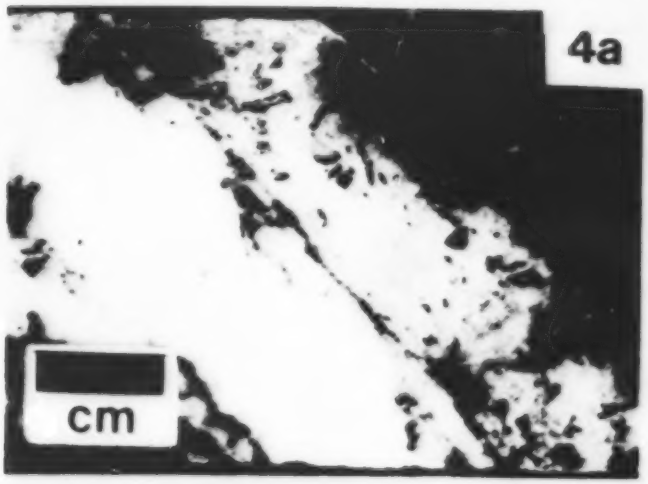

4a

4b

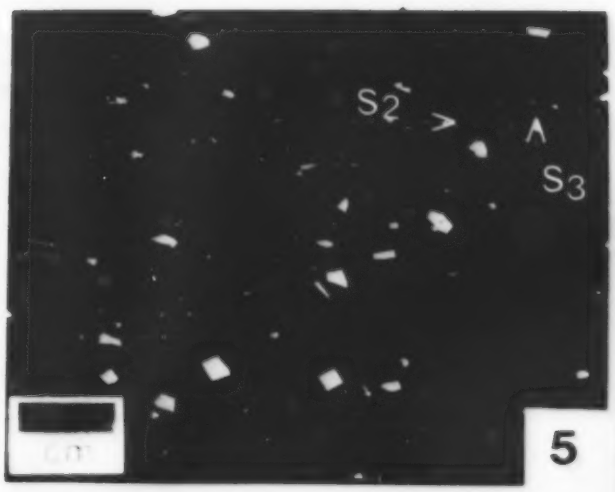

5

4c

6

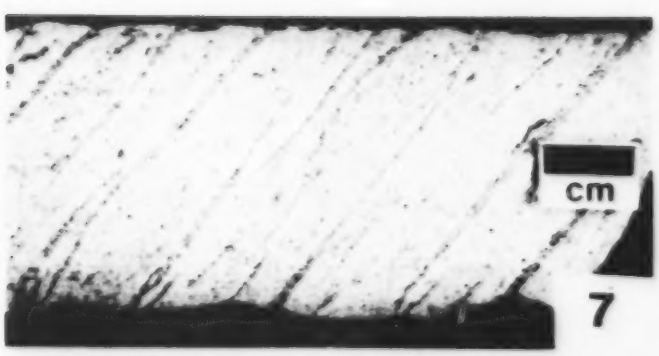

7

8. Semi-pelite hosted en echelon veins show minor F_3 folding in response to S_3 sub-horizontal crenulation cleavage within a section northwest of the Dolliver Mountain deposit. These folds plunge 8°E, roughly coincident with the plunge of the anticline in this area (10-12°E). The crenulation cleavage is axial planar to these folds. Where most intense this cleavage can deform a stratabound quartz vein into an array of en echelon veins.

9a. Specimen of D_3 deformed semi-pelite containing garnet + biotite, reflecting lower amphibolite facies metamorphism.

9b. Specimen of bleached, almost completely silicified psammite adjacent to massive quartz vein.

9c. Intensely silicified, biotite-grade psammite showing quartz-filled tension gashes cross-cutting pressure solution cleavage.

9d. Psammite wall-rock fragments within massive quartz vein showing complete replacement by chlorite + sericite.

9e. Amphibole + titanite + phlogopite + chlorite + calcite-bearing clac-silicate pod within massive quartz vein. development of such pods are likely due to wall rock interaction with high temperature fluids attending quartz veining.

9f. Amphibole + titanite + chlorite-bearing calc-silicate (skarn) band within psammite, relic pressure solution stripes are visible.

8

9a

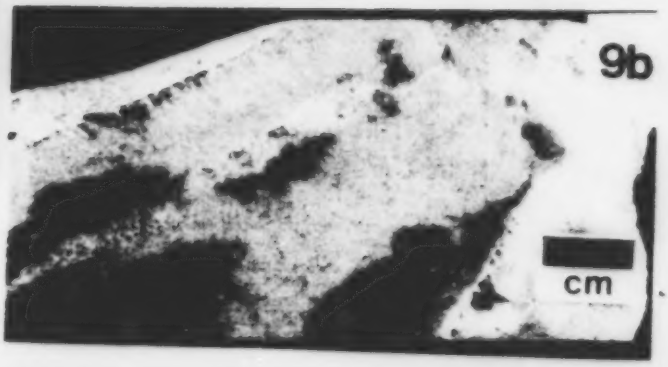

9b

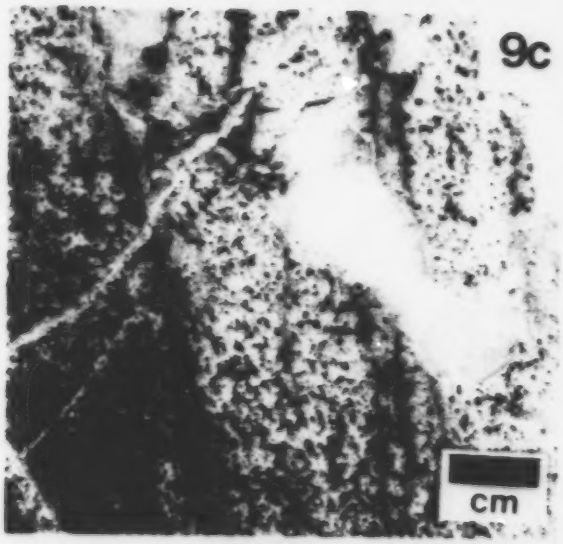

9c

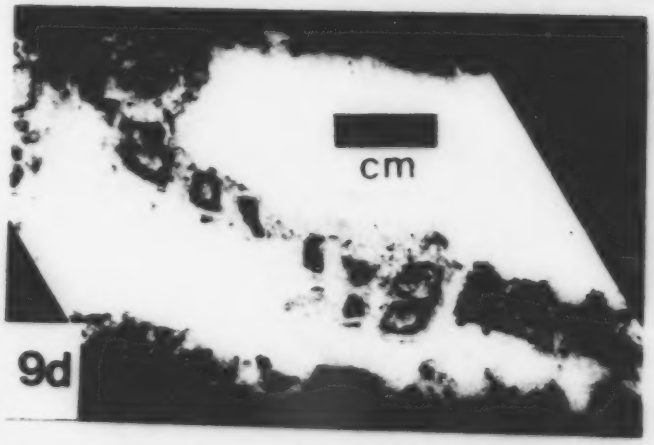

9d

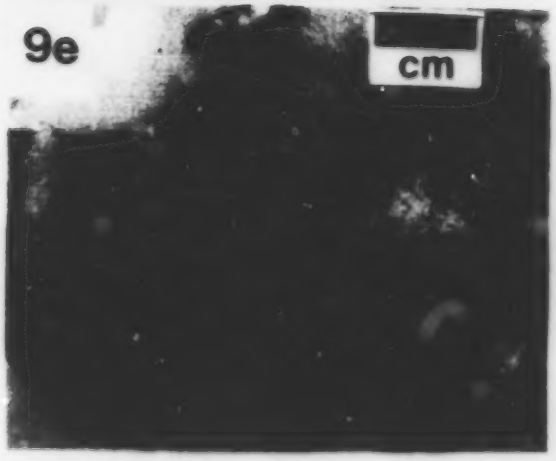

9e

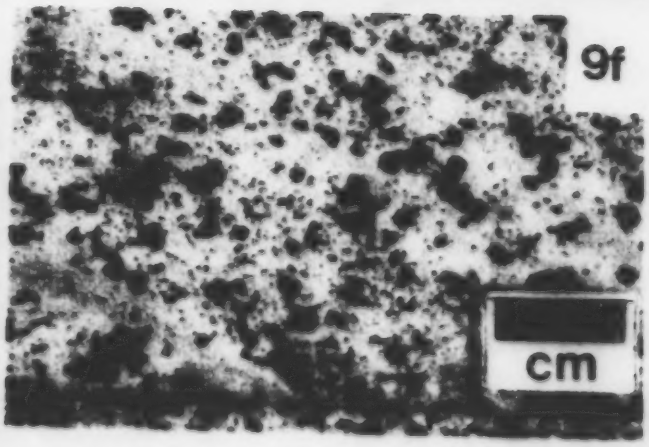

9f

9g. Specimen of granitoid pod containing coarse-grained biotite, plagioclase and quartz with minor calcite and arsenopyrite. These pods occur randomly within massive quartz veins.

9h. Coarse-grained arsenopyrite euhedra intergrown with biotite + plagioclase + calcite within a brecciated psammite.

10a. Semi-pelite showing pre-S_2 biotite grains characterized by S_2-oriented inclusions trails and commonly truncated and crenulated by S_3 cleavage. The latter is shown by the dark-grey to black lineations. Field of view = 4x7mm

10b. Close-up of 10a showing S_2-inclusion trails within ragged dark brown biotite grains and also syn -to-post-S_3 biotites which overgrow and or are oriented parallel to the subhorizontal S_3 cleavage.

10c. Pre -to syn- S_2 biotite within a fracture indicated by the penetrative S_2 cleavage and the S_2 orientation of biotite within the fracture. Field of view = 10x14mm.

10d. Biotite-filled S_3 tension-gashes. Post-S_3 biotite is indicated by the thin stringers of dark-brown biotite oriented normal to the larger lenses. Field of view = 5x7mm.

11a. Specimen showing fine-grained disseminated biotite in pelite wall rock and coarse-grained clots within a quartz vein. Field of view = 8x10mm

11b. Specimen showing similar development of biotite within quartz vein adjacent to wall rock contact. in contrast to the above however, this biotite contains chlorite + titanite. Note that away from the wall rock contact, chlorite + titanite occur without biotite. Field of view = 10x14mm.

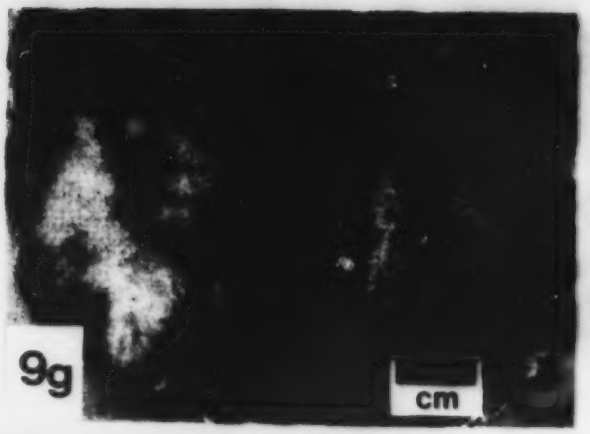
9g
cm

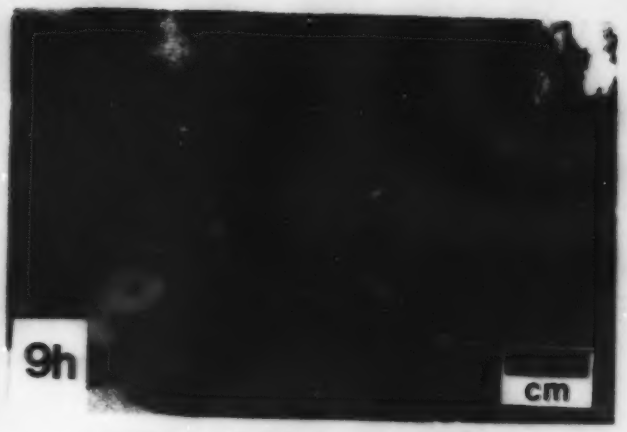
9h
cm

10a

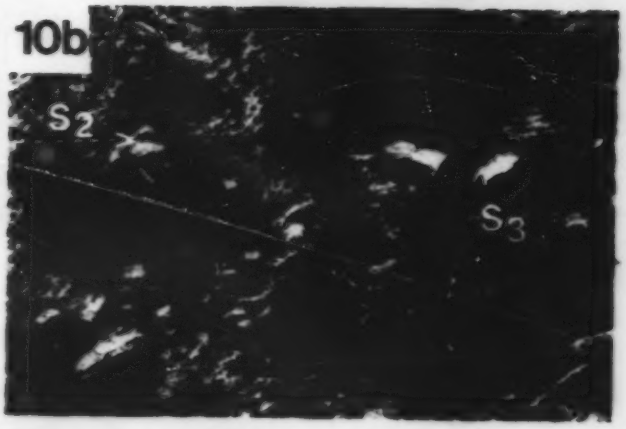
10b
S2
S3

10c

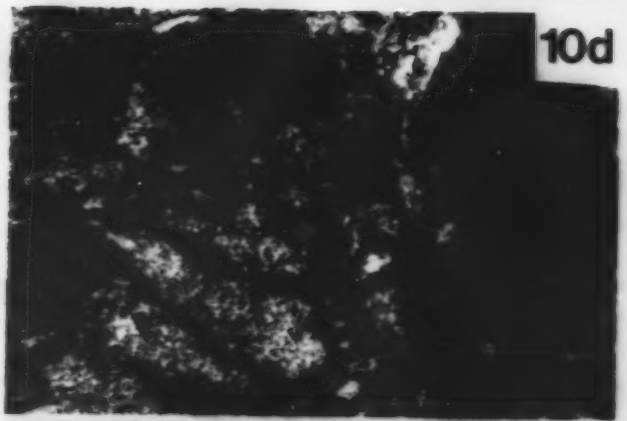
10d

11a

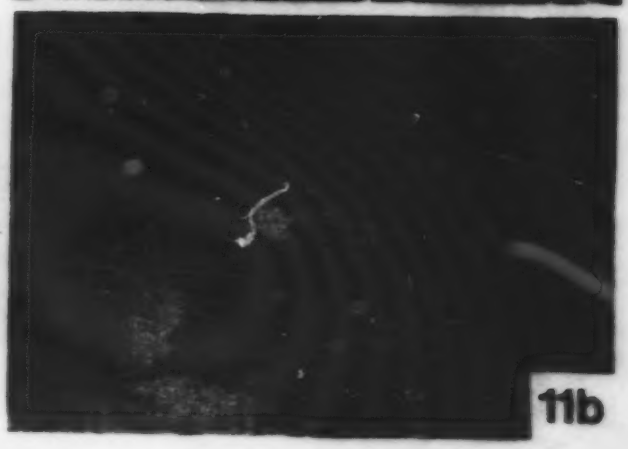
11b

11c. Fine to-coarse-grained biotite clot intergrown within pyrite and apatite within a granitic pod. Field of view = 10x14mm.

11d. Fine-grained biotite grains mantling core of quartz-sericite and chlorite. These aggregates which may represent retrograde cordierite porphyroblasts are truncated, show sinistral displacement and an en echelon arrangement in response to S_3 crenulation cleavage. Field of view = 4x7mm.

12a. Pale -to dark- brilliant green chlorite grains surrounding actinolite within a clac-silicate pod.

12b. Lenticular intergrowths of biotite + chlorite within a quartz vein and wall rock showing two preferred orientations. Note that the presence of biotite diminishes away from the wall rock. Field of view = 5x8mm.

12c. Coarse-grained aggregates of chlorite within a quartz vein, likely reflecting complete replacement of biotite.

12d. Vermicular (worm) textured chlorite grains hosted by large calcite grain within a quartz vein.

13. S_2 oriented muscovite lath within psammite matrix.

11c

11d

12a

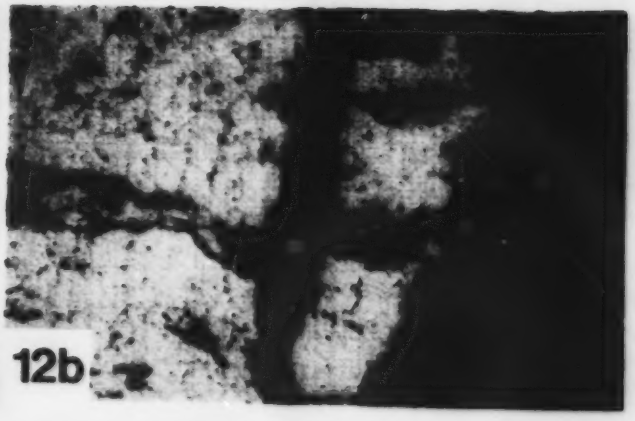

12b

12c

12d

13

14a. Plagioclase idioblasts within a silicified and sericitized pelite showing overprint by later biotite (post S_3?). field of view = 2x4mm.

14b. Close-up of plagioclase idioblast showing unusual sector twinning. 1x2mm.

14c. Plagioclase idioblasts showing altered black (graphitic?) cores and interstitial pyrite and pyrrhotite. Field of view = 5x8mm.

14d. Development of chlorite surrounded by scapolite within altered core of plagioclase grain. Field of view = 2x4mm.

15a. Optically zoned, pleochroic tourmaline crystal within psammite. Field of view = 1x2mm.

15b. Small (< 1mm), zoned tourmaline crystals associated with chlorite and titanite within a carbonitized psammite. Field of view = 1x2mm.

15c. Abundant small, acicular tourmaline crystals within an altered plagioclase grain, indicating that the minerals co-crystallized.

15d. Clot of tourmaline crystals showing pronounced basal cleavage from within a calc-silicate alteration pod.

14a

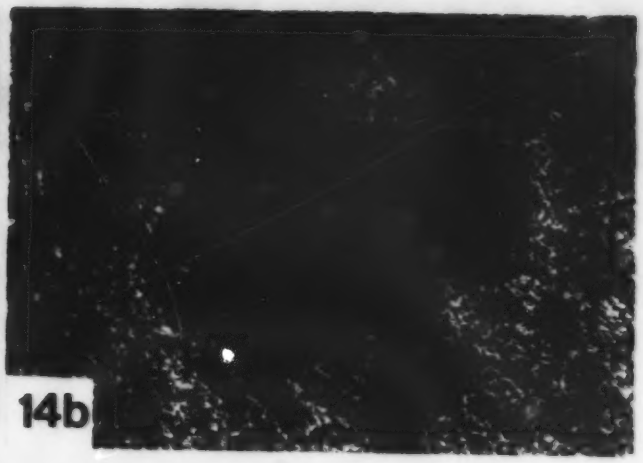

14b

14c

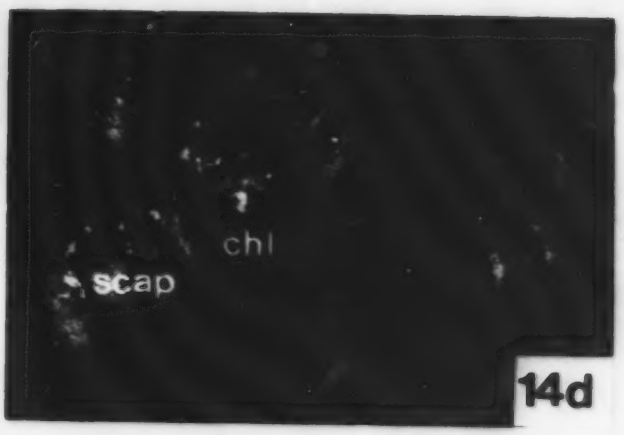

14d

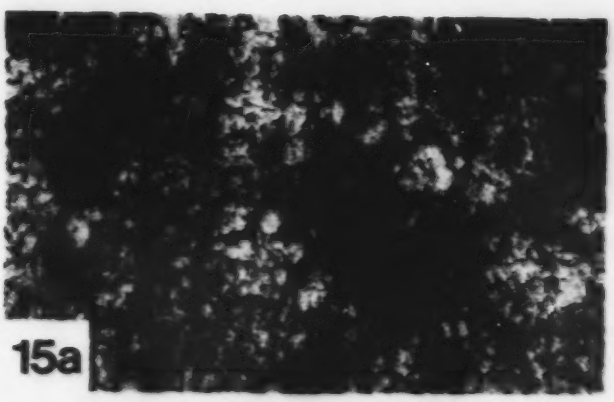

15a

15b

15c

15d

16a. Subhedral apatite grain associated withi chlorite and biotite within quartz vein adjacent to psammite wall rock. Field of view = 2x4mm.

16b. Irregular apatite grains (dark grey) within calcite. Crossed polars.

17a. Irregular grains of titanite (Ti) associated with chlorite and calcite within a calc-silicate pod. Field of view = 2x4mm.

17b. Fracture-controlled titanite grains within massive quartz vein. A partially chloritized black pelite wall rock fragment is shown to the right of the titanite. Field of view = 3x5mm.

18. Acicular clots and large crystals of actinolite and tremolite associated with chlorite and phlogopite within a calc-silicate pod. Field of view = 1x2mm.

19. Fe + Mn-rich carbonate which appears to be a pseudomorphic replacement of arsenopyrite. From within a black, graphitic pelite.

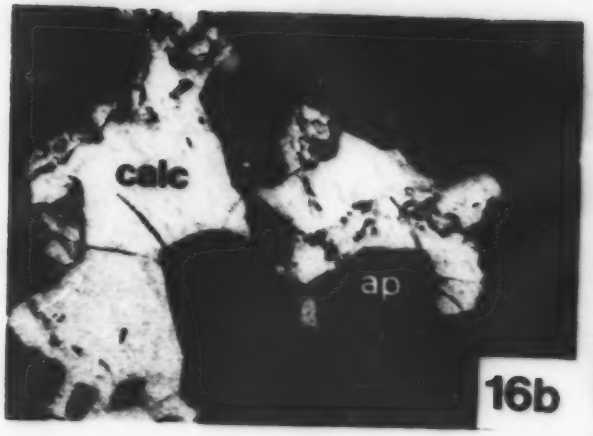

16b

16a

17a

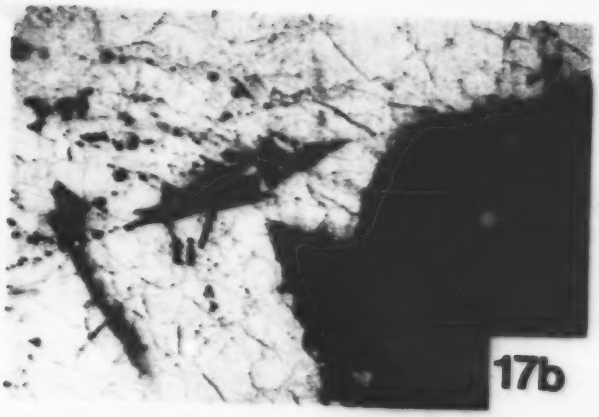

17b

18

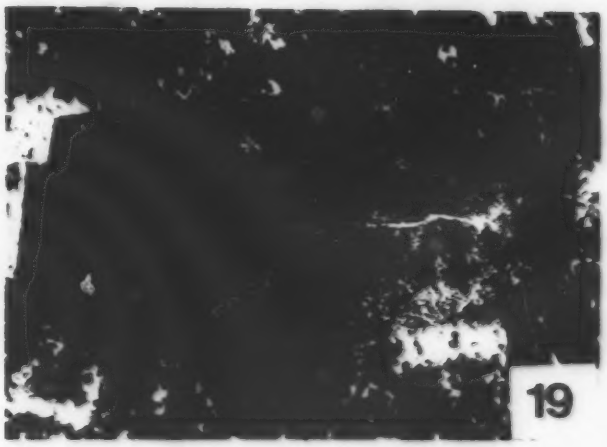

19

20a. Arsenopyrite euhedra within black, graphitic pelite showing quartz-calcite ± biotite filled pressure shadows. Field of view = 10x14mm.

20b. Large arsenopyrite crystal showing intense (D_5?) brittle deformation.

20c. Etched arsenopyrite euhedra showing well defined compositional zoning.

20d. Intergrown pyrite and chalcopyrite adjacent to arsenopyrite are cross-cut by pyrite stringer.

20e. Pyrite infilling area of intense brittle fracturing.

20f. Ilmenite blades within quartz vein at wall rock contact.

20g. Rounded rutile grains in pelite groundmass crosscut by en echelon pyrite stringers which also truncate small arsenopyrite grain.

20h. Micron-sized galena inclusion within arsenopyrite.

20a

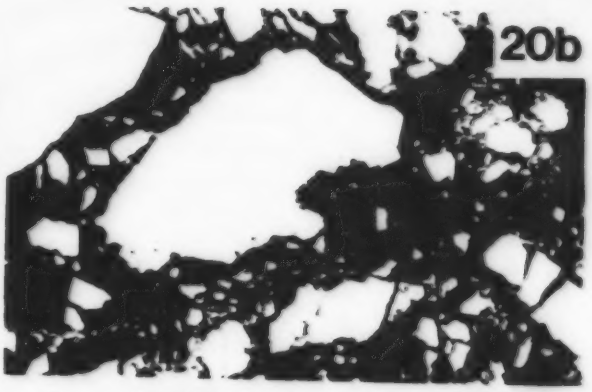
20b

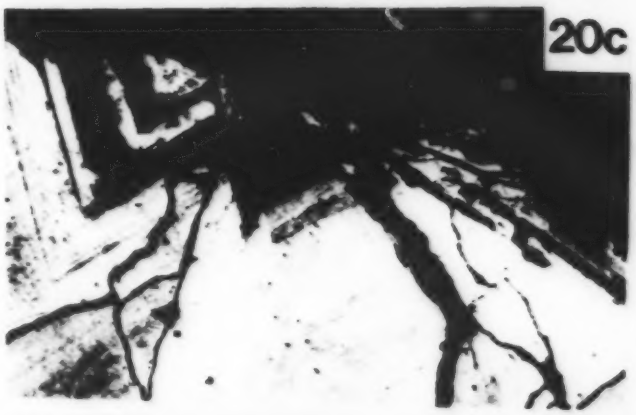
20c

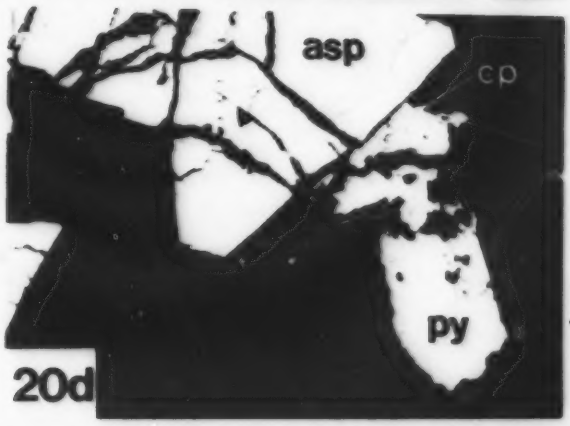

20d

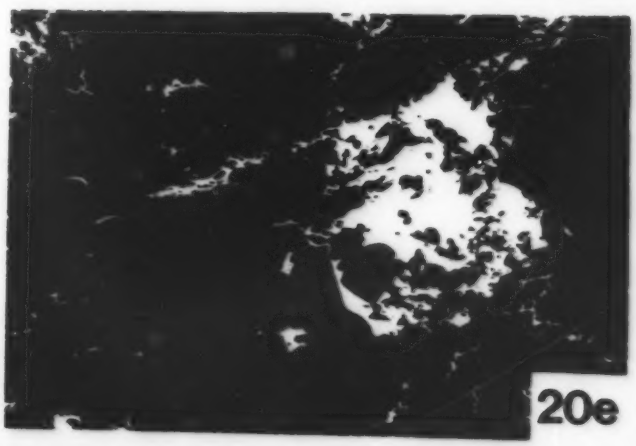
20e

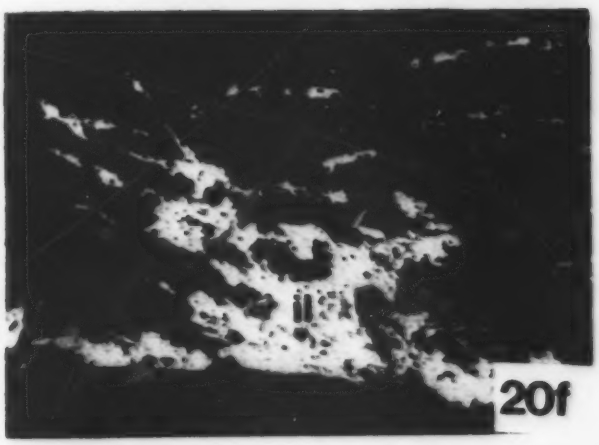
20f

20g

20h

21a. Micron-sized gold and tellurwismut (?) inclusions within arsenopyrite. Note a small inclusion of gold within the tellurismut.

21b. Irregular micron-sized inclusions of gold and galena within arsenopyrite and also larger grain of gold within pelite groundmass.

21c. Fracture-controlled gold and minor galena within arsenopyrite. Small inclusions of galena also occur within the arsenopyrite immediately above the fracture.

21d. Fracture-controlled gold and galena within arsenopyrite. The galena is Bi-rich and also contains micron-sized inclusions og gold.

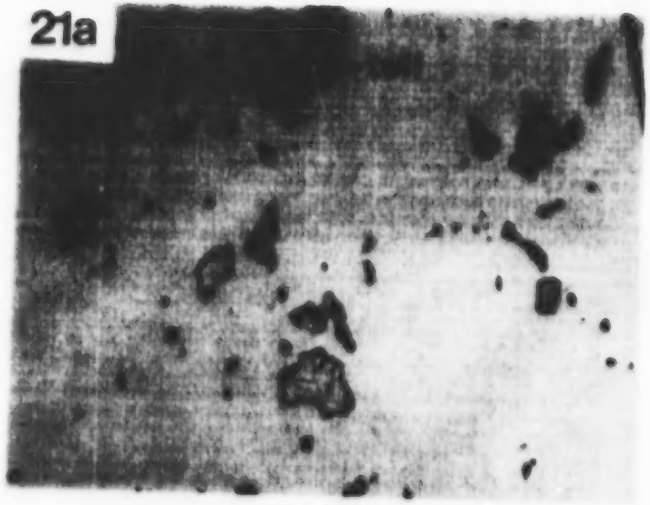
21a

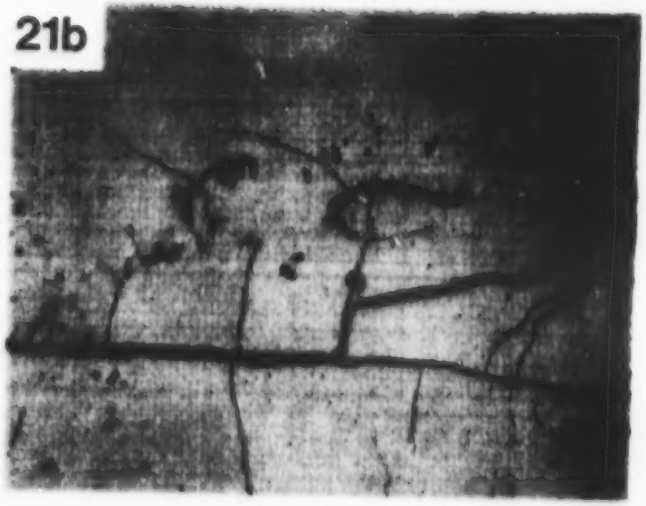
21b

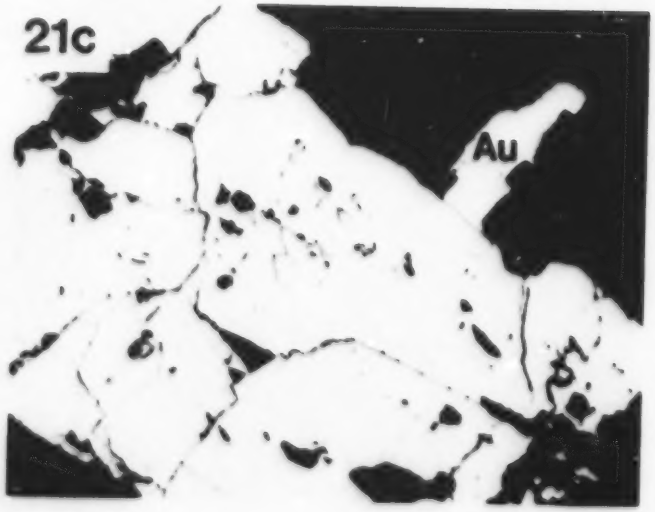
21c
Au

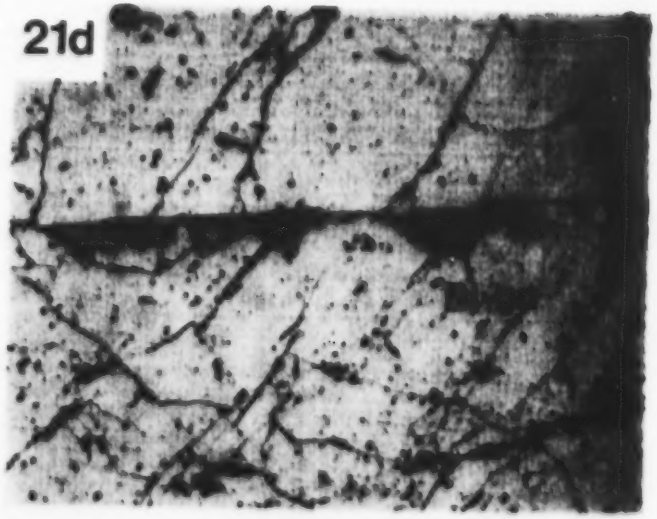
21d